Eidgenössische Technische Hochschule Zürich
Swiss Federal Institute of Technology Zurich

Bachelor Thesis

Susceptibilities in mixed-phase aerosol-cloud interaction simulated over an idealised mountain transect

Institute for Atmospheric and Climate Science, IACETH
ETH Zürich, Switzerland

Author:	Fabiola Ramelli
Supervisors:	Franziska Glaßmeier
	Prof. Dr. Ulrike Lohmann

Zürich, April 18, 2014

Supervisor: Franziska Glaßmeier
Professor: Prof. Dr. Ulrike Lohmann

Abstract

Atmospheric aerosol particles can act as CCN and IN, which catalyse the formation of cloud droplets and ice crystals, and thereby affect microphysical cloud properties. Increasing the aerosol number concentration is thought to decrease rain formation in warm-phase clouds, whereas the microphysical processes in mixed-phase clouds are more complex and uncertain.

These aerosol-induced changes in the microphysical cloud properties and the resulting changes in radiation are referred to as the indirect aerosol effect (IAE). In this study it has been disassembled in three intermediate steps: from aerosols to CCN (IN), over cloud water (cloud ice), to rain (frozen precipitation).
The influence of changes in the initial aerosol concentration on cloud and precipitation formation in orographic mixed-phase clouds is investigated in this thesis from a susceptibility perspective. The aim of this study is to analyse and to quantify the susceptibilities of these different steps of the IAE.

The atmospheric model COSMO with coupled bulk double-moment aerosol and cloud microphysics is used to conduct a pair of 2D simulations over an idealised mountain with different aerosol loads, which correspond to a clean and a polluted case. The polluted case simulation is consistent with that of *Muhlbauer et al.* [2010] for the case without flow blocking. Complementing the thesis of *Herger* [2013], this study focuses on the cold-phase processes in mixed-phase clouds.

For the susceptibility of rain to changes in the number concentration of cloud droplets a value of -0.7 is found which is consistent with the results of *Herger* [2013] and *Sorooshian et al.* [2009]. For the link between aerosols and cloud water a susceptibility of 0.9 is detected which is lower than the susceptibility value of 1.2 found by *Herger* [2013]. For the cold-phase processes, susceptibilities with magnitudes of 0.1 to 1.0 were found. There is no literature available to compare the susceptibilities of the cold-phase processes so far. However, in general, lower susceptibilities are found for the cold-phase processes compared to the warm-processes, which means that cold-phase processes are less susceptible to atmospheric aerosol perturbations.

Contents

List of Figures

List of Tables

Abbreviations

BC	black carbon
C	causes
CCN	cloud condensation nuclei
COSMO	regional climate and weather prediction model of the Consortium for Small-scale Modeling
DU	dust
E	effects
IN	ice nuclei
IAE	indirect aerosol effect
LCL	lifting condensation level
LWP	liquid water path [g/cm^2]
m_acc	mass of particles in the accumulation mixed mode
m_acc_BC_DU	mass of black carbon and dust in the accumulation mixed mode
MADE	Modal Aerosol Dynamics model for Europe
N_d	cloud droplet number concentration
SU	sulfate
OC	organic carbon
QC	mass mixing ratio of cloud water [g/kg]
QF	mass mixing ratio of frozen precipitation (snow+graupel) [g/kg]
QG	mass mixing ratio of graupel [g/kg]
QI	mass mixing ratio of cloud ice [g/kg]
QNC	number concentration of cloud droplets [# cm^{-3}]
QNI	number concentration of ice crystals [# cm^{-3}]
QR	mass mixing ratio of rain [g/kg]
QS	mass mixing ratio of snow [g/kg]
R	rain rate

Chapter 1

Introduction

Atmospheric aerosol particles play an important role in the Earth's climate system both directly by scattering and absorbing incoming solar radiation and indirectly by influencing microphysical cloud properties [*Solomon et al.*, 2007]. The cloud-active fraction of these aerosols can catalyse the formation of cloud droplets and ice crystals. Aerosol particles that are able to nucleate liquid cloud droplets are named cloud condensation nuclei (CCN), whereas particles that can initiate the formation of ice crystals are called ice nuclei (IN). The extent to which aerosols are suitable as condensation nuclei depends on different parameters like particle size, chemical composition and several ambient conditions, e.g. supersaturation [*Andreae and Rosenfeld*, 2008]. These aerosol-induced changes in the microphysical cloud properties and the resulting radiation changes are referred to as the indirect aerosol effects (IAE) [*Lohmann and Feichter*, 2005].

The first indirect effect is the cloud albedo effect which states that an enhanced aerosol concentration results in more but smaller cloud droplets, provided that the liquid water content remains constant. This leads to an increased cloud albedo [*Twomey*, 1977]. This shift in the cloud droplet size distribution towards smaller sizes is also reflected in a reduced collision-coalescence efficiency which potentially suppresses rain formation in warm-phase clouds [*Albrecht*, 1989].
The microphysical processes in mixed-phase clouds are more complex and uncertain. The riming efficiency in mixed-phase clouds may be reduced by an elevated aerosol load due to smaller cloud droplet sizes, resulting in a decreased precipitation formation rate [*Borys et al.*, 2000]. However, heterogeneous IN such as mineral dust and black carbon may counteract that effect by increasing glaciation of mixed-phase clouds which enhances the formation of snow and graupel via aggregation and riming, respectively [*Hoose et al.*, 2008].

The relationship between aerosols, clouds and precipitation has been the subject of intensive research during recent decades. However, according to the 4$^{\text{th}}$ Assessment Report of the Intergovernmental Panel on Climate Change (IPCC), the estimation of these aerosol-cloud interactions remains one of the main challenges regarding the quantification of climate feedbacks and sensitivity [*Solomon et al.*, 2007].

In this thesis, we investigate the influence of aerosol particles on precipitation formation in mixed-phase orographic clouds from a susceptibility perspective. Orographic clouds form as moist air is forced above the lifting condensation level (LCL) due to a surface elevation where condensation occurs [*Roe*, 2005]. It has proven difficult to quantify the IAE on precipitation in mixed-phased clouds, due to the above mentioned complex microphysical processes in these clouds [*Denman et al.*, 2007].

The aim of this study is to analyse and to quantify the susceptibility of (a) different microphysical processes proceeding in mixed-phase orographic clouds and (b) orographic precipitation to changes in the atmospheric aerosol concentration using computer simulations with explicit mixed-phase aerosol-cloud-precipitation interactions. We take the approach to disassemble the susceptibility of precipitation on aerosol in intermediate steps: (1) susceptibility of CCN/IN to modification of the aerosol concentration, (2) susceptibility of cloud water (cloud ice) to changes in the amount of CCN (IN), (3) susceptibility of precipitation (frozen precipitation) to changes in the number concentration of cloud droplets (cloud droplets/ice crystals). The idea behind this concept is to identify the determining step along the aerosol-to-precipitation-path and to investigate the response of microphysical processes on anthropogenic aerosol perturbations.

This concept was also used in the thesis of *Herger* [2013], where she analysed susceptibilities in mixed-phase clouds with different aerosol concentrations over an Alpine transect (Jungfraujoch), focusing on warm-phase processes. Complementing her study, in the following we will especially examine the importance of the ice phase for the IAE on precipitation. Since *Herger* [2013] reports some difficulties with the Jungfraujoch model setup and orography is considered as a major factor for inducing and enhancing precipitation [*Roe*, 2005], in the present study an idealised mountain setup is applied. One advantage of this simplified 2D model setup is that it is possible to define a single flow regime for the whole computational domain, while in the Jungfraujoch setup the flow regime is not clearly defined. This setup provides simplified atmospheric dynamics and thus simplifies the examination of susceptibilities.

The atmospheric model of the Consortium for Small-Scale Modelling (COSMO) with coupled bulk double-moment aerosol and cloud microphysics was used to conduct a pair of 2D simulations over an idealised mountain by changing aerosol initial concentrations (clean, polluted). The polluted case simulation is consistent with that of *Muhlbauer et al.* [2010] for the case without flow blocking.

The theoretical basis for this study is given in chapter 2. Chapter 3 provides information on the model setup and evaluation. In chapter 4 the results of the different simulations are presented and discussed within the scientific context. To conclude, a critical reflection of this study and an outlook for further studies is provided in chapter 5.

Chapter 2

Theory

In the first part of this chapter, the different aerosol indirect effects are discussed briefly. The fundamental microphysical processes proceeding in mixed-phase clouds are explained in the second section. Finally, an overview of the susceptibility concept which is applied for this study is given.

2.1 Indirect aerosol effects

Aerosol particles can influence cloud properties and precipitation in several ways, acting either as CCN or IN, or as absorbing particles. These aerosol-cloud-precipitation interactions can be divided into different effects [*Solomon et al.*, 2007].

The cloud albedo effect was first proposed by *Twomey* [1977]. It comprises the idea that an enhanced aerosol concentration leads to an increase in aerosols acting as CCN and therefore to more but smaller cloud droplets, provided that the liquid water content remains unchanged. The consequence is a higher cloud reflectivity.
This shift in the cloud droplet size distribution towards smaller sizes reduces the collision-coalescence efficiency and thus potentially decreases precipitation formation in warm-phase clouds, resulting in an increased cloud lifetime. This effect is referred to as the cloud lifetime effect [*Albrecht*, 1989].
However, in mixed-phase clouds, the glaciation indirect effect can partially offset the cloud life time effect [*Lohmann and Diehl*, 2006]. This is due to the fact that an elevated aerosol load implies not only a higher CCN concentration, but also an increased number of aerosols serving as IN. This leads to a rapid glaciation of supercooled clouds since the saturation vapour pressure over ice is lower than the saturation vapour pressure over water. Thus, in an ice super-saturated environment, ice crystals grow rapidly at the expense of cloud droplets inducing a higher amount of precipitation via the ice phase. This process is named after their discoverers, Bergeron-Findeisen process [*Lohmann*, 2002].

Figure 2.1 shows the cloud albedo and the cloud lifetime effects in warm-phase clouds (left column) and the glaciation indirect effect in mixed-phase clouds (right column).

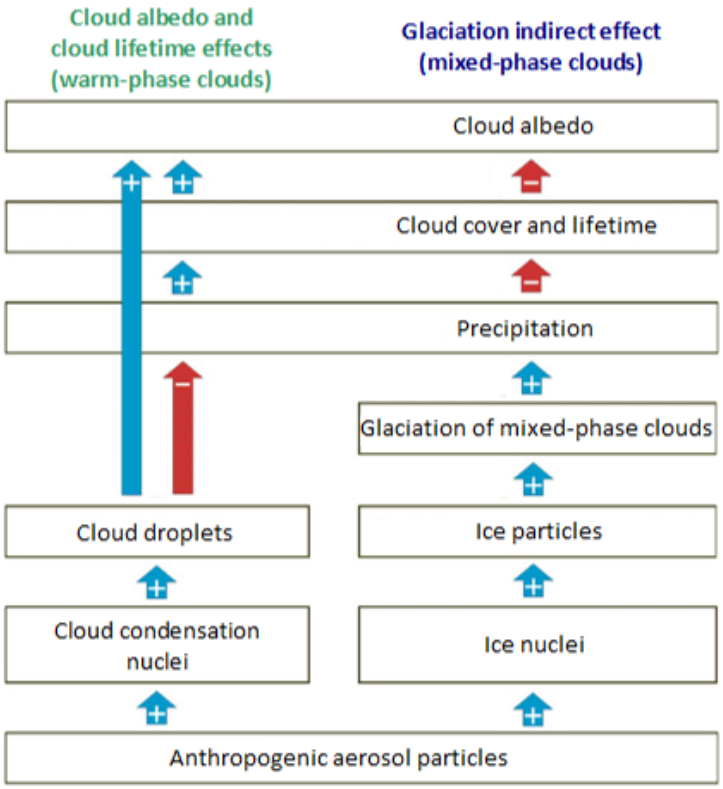

Figure 2.1: **Indirect aerosol effects**: The left column shows the cloud albedo and the cloud lifetime effects in warm-phase clouds. The glaciation indirect effect in mixed-phase clouds is illustrated on the right-hand side. Blue arrows indicate positive correlations, whereas red arrows mark negative relations. Adapted from *Hoose et al.* [2008].

2.2 Processes

In this section some essential processes along the aerosol-to-precipitation-path are discussed. Here we restrict ourselves to the examination of the ice-phase processes. For information about the warm-phase processes we refer to *Herger* [2013].
Firstly, some theoretical background on heterogeneous ice nucleation is given. In the following step, we focus on the criteria which are thought to be important for aerosols to act as IN. Finally, the growth processes of ice crystals to precipitation-size hydrometeors are discussed.

2.2.1 Heterogeneous ice nucleation

Pure water droplets in the atmosphere are known to supercool to about -38 °C before they freeze homogeneously [*Koop et al.*, 2000]. Homogeneous ice nucleation is important mainly in the upper altitudes of the troposphere. Suitable aerosols with favourable surface properties can act as IN, catalysing ice formation at higher temperatures. Heterogeneous ice nucleation is the dominant freezing process in mixed-phase clouds. It requires the presence of an IN which reduces the energy barrier to the formation of a critical ice germ relative to homogeneous nucleation. This factor between homogeneous and heterogeneous nucleation is a function of the contact angle. The lower the contact angle, the better the ice nucleation ability of the substrate since fewer water molecules are required for the formation of a critical ice germ [*Lohmann and Lüönd*, 2012].

Four different freezing modes have been proposed in the literature: (1) deposition nucleation (2) immersion freezing, (3) condensation nucleation and (4) contact freezing. An overview of the different freezing mechanisms is given in figure 2.2. Immersion freezing is the only ice nucleating process considered in the Jungfraujoch setup, while the idealised mountain setup takes into account all nucleation modes via an empirical parametrisation [*Bangert*, 2012]. Deposition nucleation describes the direct deposition of water vapour onto an ice nucleus. Immersion freezing refers to the freezing process that is initiated by an IN within a supercooled water droplet. In contrast, if the aerosol containing the IN starts from a subsaturated environment the process is known as condensation nucleation. Contact freezing includes the collision of an IN and a supercooled cloud droplet [*Lohmann and Lüönd*, 2012].

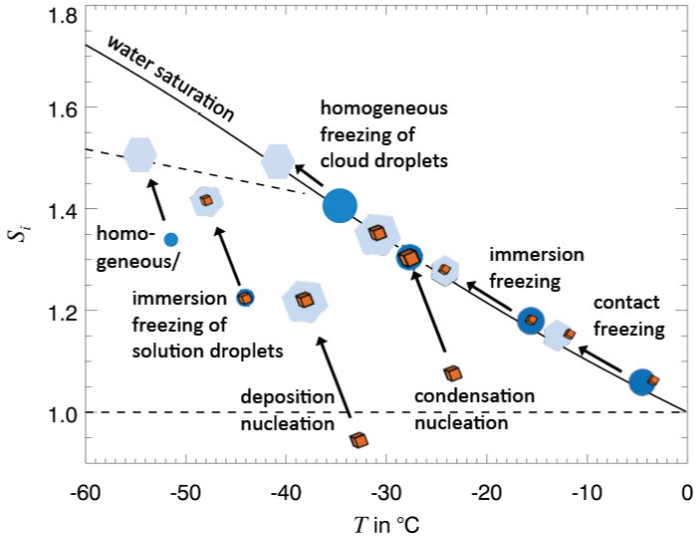

Figure 2.2: **Nucleation modes** : Overview of the different ice nucleation modes: (1) deposition nucleation, (2) immersion freezing, (3) condensation nucleation and (4) contact freezing. In this study all nucleation modes are taken into account. From *Hoose and Möhler* [2012].

2.2.2 Requirements for effective ice nucleation particles

Only a small fraction of the aerosol particles in the atmosphere can serve as IN. The IN concentration varies between values of 10^{-4} and $10^{-1}\,\mathrm{cm}^{-3}$ which is some orders of magnitudes lower than those of CCN [*Pruppacher and Klett*, 1997].

The criteria for aerosols to act as IN are more uncertain compared to those of CCN. According to *Pruppacher and Klett* [1997] the requirements for aerosols to be an effective IN are thought to be:

- solid state: provides a surface for the formation of an ice germ
- insolubility: water absorption may cause the substrate to decay
- particle size: larger particles are more effective IN
- crystalline structure: structure similar to ice may increases the ice nucleation ability
- molecular bindings with water: good IN should be able to form H-bonds with water
- active sites: the energy barrier is particularly small in cracks

However, there is controversy over the importance of these criteria and, so far, it is not possible to make predictions about the ice nucleation ability of a substrate on the basis of its chemical and physical properties [*Pruppacher and Klett*, 1997].

2.2.3 Growth processes of ice-phase hydrometeors

Ice crystal growth by diffusion

As discussed in section 2.1, in mixed-phase clouds, a newly formed ice crystals is in an ice-supersaturated environment. Under these conditions, ice crystals grow rapidly by diffusion at the expense of cloud droplets. Ice crystals may even reach precipitation size by diffusion which is not possible for cloud droplets. Thus, growth by diffusion is more important for ice crystals compared to water droplets.

Ice crystal growth by collision-collection

In mixed-phase clouds, the collision-collection process is more complex than the collision-coalescence process in warm-phase clouds since there are different possibilities depending on the involved particles: An ice crystal can collide and stick together with another ice crystal forming an aggregate or a snowflake. This process is referred to as aggregation.
Riming is observed when an ice crystal or snowflake collides with a supercooled cloud droplet that freezes upon contact. If the freezing occurs immediate, this process results in the creation of graupel.
Collision of a cloud droplet or an ice crystal with a precipitation-size hydrometeor is called accretion. It is caused by the difference in fall velocity between the large collector particle and the smaller captured particle [*Lohmann and Lüönd*, 2012].

2.3 Susceptibility concept

The aim of this study is to investigate the aerosol-cloud-precipitation interactions in mixed-phase clouds, in order to improve the understanding and the quantification of the indirect aerosol effect. The main question is to determine how a change in the aerosol abundance affects cloud and precipitation formation. In this study, this is carried out by means of a susceptibility perspective. The susceptibility concept was proposed by *Feingold and Siebert* [2009] in a study, where they established a measure to investigate the extent to which precipitation is influenced by changes in the cloud droplet number concentration. This sensitivity of rain to changes in the number density of cloud droplets is referred to as the precipitation susceptibility and given by the following equation

$$S_0 = -\frac{d\ln R}{d\ln N_d} \tag{2.1}$$

where R is the rain rate and N_d the cloud droplet number concentration. The minus sign reflects the fact that aerosol concentration and rain are negatively correlated in the warm-phase case (lifetime effect). Larger values of S_0 indicate a higher sensitivity of rain to changes in N_d.

In this study, we extend the precipitation susceptibility concept suggested by *Feingold and Siebert* [2009] as it has also been done by *Quaas et al.* [2009], replacing R and N_d by different cloud properties. The idea behind this is to consider also the susceptibility of the previous steps: from aerosol to CCN (IN), over cloud water (cloud ice) to rain (frozen precipitation). Instead of directly calculating the susceptibility of precipitation to changes in the aerosol abundance, we take the approach to disassemble the IAE in three intermediate steps, which are shown in figure 2.3.

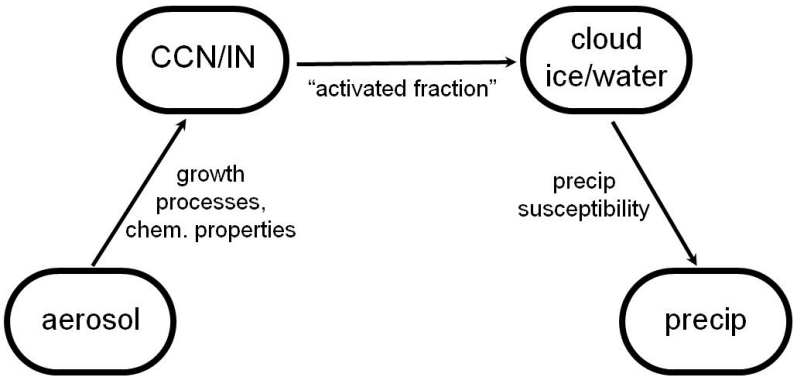

Figure 2.3: **Susceptibility concept**: The IAE is divided into three steps. Susceptibilities are calculated for every single step of the IAE. In this study we focus on the cold-phase processes. Courtesy of Franziska Glaßmeier.

The first step corresponds to the susceptibility of CCN (IN) to changes in the aerosol load. The following step describes the susceptibility of cloud water (cloud ice) to changes in the CCN (IN) concentration. Finally, the susceptibility of rain (frozen precipitation) to cloud droplets (cloud droplets/ice crystals) is examined. The idea behind this breakdown of the IAE in single steps is to try to identify the determining step along the aerosol-to-precipitation path and to investigate the response of microphysical processes on anthropogenic aerosol perturbations. In this study we focus primarily on the cold-phase processes.

The susceptibility concept can be extended by generalising equation (2.1) to the following form:

$$S = \frac{dE/E}{dC/C} = \frac{d\ln E}{d\ln C} \tag{2.2}$$

where E indicates the effect and C the cause. In contrast to *Stevens and Feingold* [2009], we have not applied a minus sign on the definition of the susceptibility. This means that we need to regard the absolute values of the susceptibilities in order to compare them to other studies.

For our calculations we used the following equation, which is deduced from the first order Taylor approximation of equation (2.2):

$$\frac{\Delta E/E}{\Delta C/C} \approx \frac{\Delta \ln E}{\Delta \ln C} \tag{2.3}$$

To illustrate the meaning of S, assume the idealised case that an effect E can be linked to a cause C by a power law function

$$E(C) = a \cdot C^{\alpha} \tag{2.4}$$

where a is a constant. If we insert equation (2.4) in equation (2.2) we obtain the following relation:

$$S = \frac{dE/E}{dC/C} = \frac{d\ln E}{d\ln C} = \frac{d(\ln(a \cdot C^{\alpha}))}{d\ln C} = \frac{d(\ln a + \ln C^{\alpha})}{d\ln C} = \frac{d(\ln a + \alpha \ln C)}{d\ln C} = \alpha \tag{2.5}$$

Thus, the exponent α corresponds to the susceptibility S.

There is also the possibility to interpret this relationship in a graphical manner. For that purpose, the natural logarithm of equation (2.4) is calculated which yields:

$$\ln E = \ln(aC^{\alpha}) = \ln a + \alpha \ln C \tag{2.6}$$

If we replace $\ln E$ by y, $\ln a$ by c and $\ln C$ by x, we get a linear function of the form

$$y = c + \alpha x \tag{2.7}$$

A schematic of equation (2.6) is given in figure 2.4.

For each step of the IAE a susceptibility value could be obtained by creating a log-log plot of pairs (lnC, lnE) for each single point in the computational domain and then performing a linear regression. The resulting slope corresponds to the mean susceptibility over the simulated area. This is typically performed for satellite data (e.g. *Quaas et al.* [2009]).

Instead of relying on the variability within one simulation, another approach is used in the present study: the susceptibility of a particular step in the IAE is determined by calculating susceptibilities for each point within the computational domain and then computing the geometric mean of these single susceptibility values over a specific area. This approach will be further discussed in chapter 3.

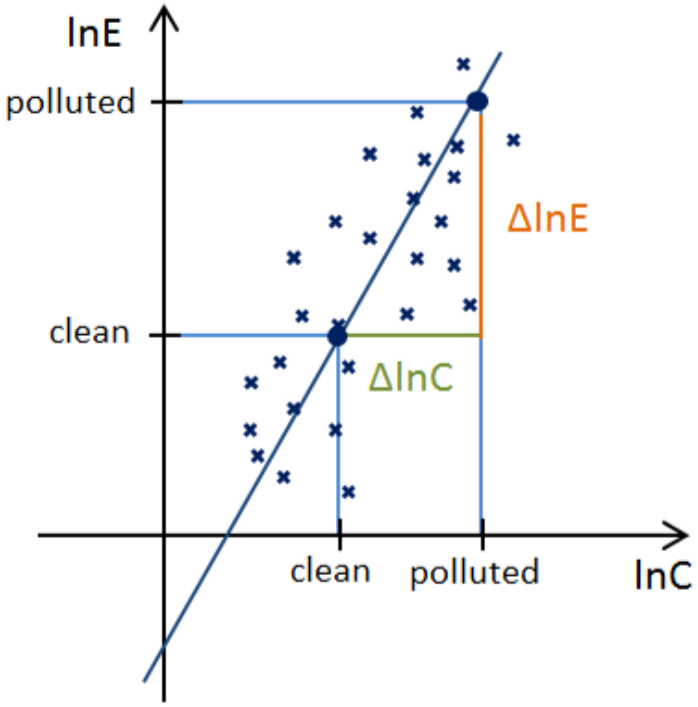

Figure 2.4: **Power law function**: Effect E is linked to the cause C by a power law function. A linear regression is performed for the single data points. The slope of the straight line corresponds to the susceptibility.

Chapter 3

Method

In the first part of this chapter, the numerical model used in this study is briefly described. This chapter provides also specifications on the model setup which is applied for the different simulations. In the last section, fundamental equations concerning this study are presented.

3.1 Model description

In this study, we used the non-hydrostatic atmospheric model of the Consortium for Small-Scale Modeling (COSMO) with coupled bulk double-moment aerosol and cloud microphysics. As we focus primarily on microphysical processes, aerosol-radiation interaction and related feedbacks were neglected in the model setup. For further information on the setup of the COSMO model we refer to [*Zubler et al.*, 2011].

3.1.1 Microphysics of aerosols

The Modal Aerosol Dynamics model for Europe (MADE) is coupled to the COSMO model in order to simulate atmospheric chemical composition, number concentration and size distribution of submicrometer aerosols. The aerosol size distribution is represented by four overlapping log-normally distributed modes.

In this study we focus on black carbon (BC), organic carbon (OC), sulphate (SU), dust (DU) and aerosol liquid water (H_2O) in the Aitken and Accumulation mode. The contribution of nitrate (NO_3) and ammonium (NH_4) is zero. No condensation and thus coating by sulphuric acid is considered. The schematic in figure 3.1 gives an overview of the filled modes.
The MADE aerosol model considers emission from aerosol sources and models the atmospheric aerosol particles concentration through coagulation, condensation, transport and deposition. The inclusion of removal processes is a huge progress compared to the aerosol module M7 which is used for the Jungfraujoch transect. We refer to *Vogel et al.* [2009] for further information on the MADE aerosol model.

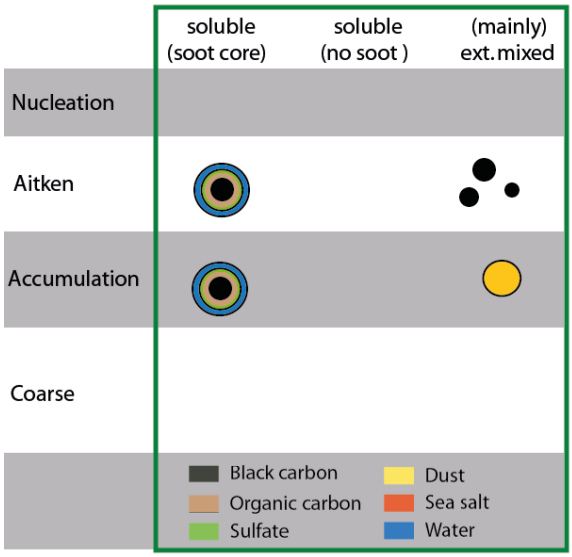

Figure 3.1: **Aerosol microphysics module MADE**: This schematic gives an overview of the considered modes. The following modes are filled: Aitken and Accumulation mixed, Aitken soot and Accumulation dust. Slightly adapted from F. Glassmeier (private communications).

3.1.2 Microphysics of clouds

The activation process is parameterised as in *Fountoukis and Nenes* [2005] (for details please consult *Bangert* [2012].
Cloud microphysical processes are considered with a two-moment bulk scheme from *Seifert and Beheng* [2006], which is coupled to the MADE aerosol model. Hydrometeors are classified in five categories: cloud droplets, ice crystals, rain, snow and graupel. Table 3.1 gives an overview of the warm- and ice-phase microphysical processes included in the scheme. Aggregation and riming are the most important cold-phase microphysical processes in this study. They are responsible for the formation of snow and graupel. For further information about the parameterisation of the microphysical processes, we refer to *Seifert and Beheng* [2006].

warm-phase microphysical processes	cold-phase microphysical processes
nucleation of cloud droplets	heterogeneous nucleation
condensation/evaporation of cloud droplets	sublimation/melting/freezing
autoconversion of cloud droplets to rain	riming/aggregation
self-collection of cloud droplets and rain	collection
breakup of large rain drops	secondary ice nucleation

Table 3.1: **Warm- and cold-phase microphysical processes in mixed-phase clouds**

3.2 Model setup

3.2.1 Computational domain

For this study, we use a two-dimensional setup over an idealised mountain with 60 vertical model levels. The size of the computational domain is 21 km in the vertical direction and 880 km in the horizontal direction. The horizontal is divided in 400 intervals with a grid point spacing of 2.2 km. For this study, data is given for 32 height levels. The idea of this model setup is to simulate the aerosol-cloud-precipitation interactions on a high resolution scale.
A time step of 10 seconds is applied in all simulations, while the output is written every 15 minutes. The output represents a snapshot and does not provide a mean value of the respective 15-minute interval. The COSMO model is not able to issue the output more frequently. The run duration of each simulation is 10 hours.

3.2.2 Topography

In order to control the influence of topography on the formation of orographic clouds and precipitation, we used an idealised mountain. The idealised mountain is parametrised with the following equation from *Muhlbauer et al.* [2010]

$$h(x) = \frac{h_0}{16}\left(1 + cos\left(\pi\frac{x - x_0}{4a_0}\right)\right)^4 \tag{3.1}$$

where h_0 is the maximal height of the mountain at the position x_0 (centre of the field of observation) and a_0 indicates the half width of the mountain. We set h_0 to 1000 m, x_0 to 440 km and a_0 to 30 km for all simulations. The motivation behind this mountain shape is to generate a flow regime without flow blocking. The specification of the flow regime is one advantage of the idealised mountain setup compared to the Jungfraujoch setup where the dynamical flow processes are complex and uncertain.

3.2.3 Simulations

A series of simulations are performed to examine the sensitivity of different microphysical processes on aerosol perturbations. The aerosol abundance varies between the different setups. An overview of the different simulations is given in table 3.2.

Simulation	T(K)	aerosol
SIM_cc	273	clean
SIM_cp	273	polluted

Table 3.2: **Parameter specifications for the idealised set of simulations**

SIM_cc and SIM_cp are conducted with a sea-level temperature of 273 K. The aerosol concentration differs between the simulations. SIM_cc is prescribed as the clean case and SIM_cp as the polluted case. The polluted aerosol setup follows *Weingartner et al.* [1999]. The aerosol number and size distribution of the polluted case are shown figure 3.2. The clean case is constructed by multiplying the polluted case distribution by a factor of 0.3.

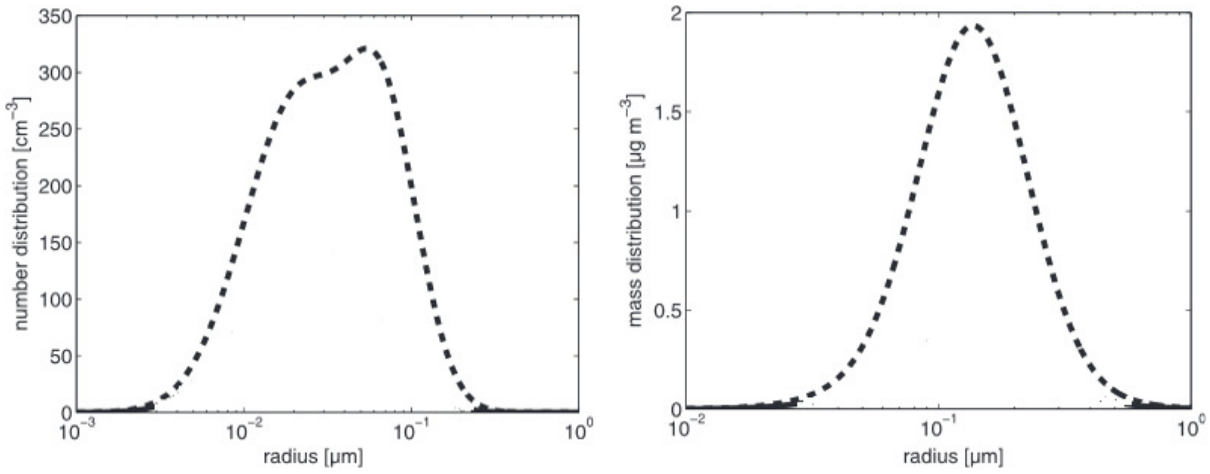

(a) (b)

Figure 3.2: **Aerosol number and size distribution of the polluted simulation**: The aerosol number (left) and size (right) distribution of the polluted case are consistent with those of *Weingartner et al.* [1999]. The clean case is constructed by multiplying these distributions by a factor of 0.3. Adapted from *Muhlbauer et al.* [2010]

3.2.4 Meteorological initial and boundary conditions

The initial vertical profiles of horizontal wind speed and relative humidity are shown in figure 3.3. The horizontal wind speed is 15 m/s within the first 10 km, increases linearly to 40 m/s at an altitude of 21 km and remains constant at 40 m/s within the last kilometre. The relative humidity at the surface is 0.95 and decreases linearly to 0.78 at an altitude of 5 km, to 0.2 at a height of 7 km, and finally to 0.03 at 12 km. Above 12 kilometre the relative humidity is kept constant at a value of 0.03, which means that the atmosphere is very dry around these levels.
The moist Brunt-Väisälä frequency is a measure for the atmospheric stability. It is kept constant at a value of 0.01 along the whole vertical profile. This stable stratification of the atmosphere is important, since we consider only orographic induced uplift and do not study processes like convection.
These profiles are also used as boundary conditions at the sides during the simulation.

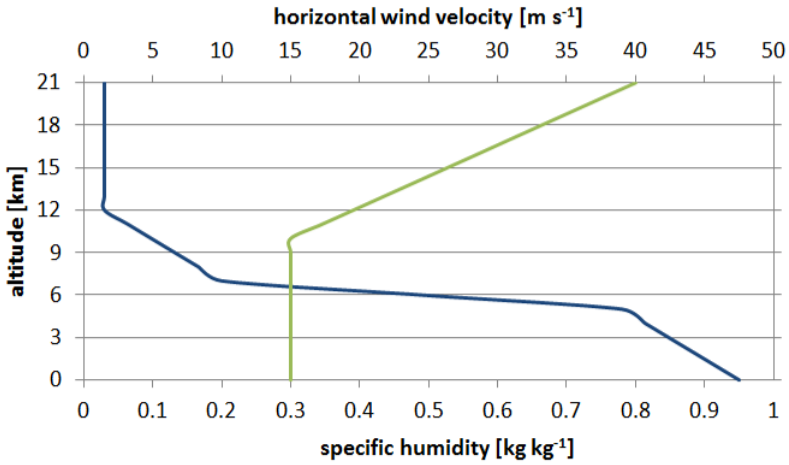

Figure 3.3: **Vertical profiles of meteorological initial conditions**: Initial vertical profiles of horizontal wind velocity (green) and specific humidity (blue) for SIM_cc and SIM_cp.

3.2.5 Time versus ensemble average

There are different possibilities to create an average. The approach of the time average is applied for the idealised mountain setup. It is the averaged quantity of a single system over a certain time interval. On the contrary, the ensemble average is used for the Jungfraujoch setup. The ensemble average is the averaged quantity of many similar systems, in our case weather situations, at a certain time. The consideration of many different initial conditions and thus weather situations is one advantage of the ensemble average compared to the time average which corresponds to a specific weather situation.
Hence, the two approaches corresponds to the mean over different time scales. The time mean averages over minutes, whereas the ensemble mean corresponds to the average over a time scale of hours or days.

3.3 Formulas

Relative difference
The relative difference describes the relative change of a variable between the clean and polluted case as a function of latitude and altitude (x, h), averaged over a specific period of time. The field considered are aerosol species, CCN, IN, cloud water, cloud ice and different forms of precipitation-size hydrometeors (rain, snow, graupel). The general equation is given as follows:

$$\frac{\Delta f}{f}(x,h) = \frac{\overline{f_{polluted}(x,h)} - \overline{f_{clean}(x,h)}}{0.5(\overline{f_{polluted}(x,h)} + \overline{f_{clean}(x,h)}} \tag{3.2}$$

The relative difference assumes values between -2 and 2. A positive value indicates that the corresponding parameter is higher in the polluted case compared to the clean case. In contrast to the Jungfraujoch setup, we don't use the Wilcoxon rank-sum test to test if the difference between the clean and polluted case is significant, but we apply a threshold value for the different quantities which are described in section 4.2.

Susceptibilities
The susceptibility concept has been explained in section 2.3. Equation (3.3) describes the susceptibility of an effect E to changes in the cause C as a function of latitude and height (x, h) averaged over a specific time interval.

$$\frac{\Delta \ln E}{\Delta \ln C}(x,h) = \frac{\ln \overline{E_{polluted}} - \ln \overline{E_{clean}}}{\ln \overline{C_{polluted}} - \ln \overline{C_{clean}}} \tag{3.3}$$

As for the relative differences, susceptibilities are only calculated when the different quantities are above a specific threshold value.

Geometric average
In order to quantify the relative differences and the susceptibilities over a specific region, we determine the geometric mean over this area using the following formula

$$\langle x_{geomean} \rangle = \sqrt[n]{x_1 x_2 x_3 ... x_n} \tag{3.4}$$

where n is the number of grid points and x the values of the data points within the considered area. Geometric means are usually used for rates and susceptibilities can be regarded as rates.

Chapter 4

Results and discussion

In the first part of this chapter, the adjustment to the steady state is discussed. The second part gives an overview of the different hydrometeors within the domain and thus on the location of the clouds. The threshold values applied in this study are also described in this section. Finally, susceptibilities are determined for the different steps of the IAE and compared to other studies.

4.1 Adjustment to the steady state

As already mentioned, the time average is applied for the idealised mountain setup. In order to determine the time period over which the different quantities are averaged, we have to identify the onset of the steady state. We assume that the steady state is achieved as soon as the dynamical parameters in the atmosphere reach a constant level (e.g. specific humidity, horizontal/vertical wind velocities). The maximum values as well as the domain averages of specific humidity (QV), horizontal (U) and vertical wind speed (W) can be found in A.1. Absolute values and relative differences of QV, U and W are also displayed there.
However, some hydrometeor variables do not reach their steady state within the simulation time of 10 hours. As an example the integrated time average over the whole computational domain of snow (QS) is shown in figure 4.1. The integrated time average of further hydrometeors can be found in A.2. The red area indicates a sector where a relatively constant progression is recorded for all moisture variables. This area corresponds to the time period between t=4.5 h and t=7.5 h.
Hence, instead of determining the adjustment time of the steady state by considering dynamical parameters, we identify a time period where all moisture variables have a nearly constant course. This period is assumed to be comparable with a steady state situation. Thus, all quantities in the course of this study are averaged over a time period of 3 hours, namely between t=4.5 h and t=7.5 h (of $t_{end} = 10$ h).

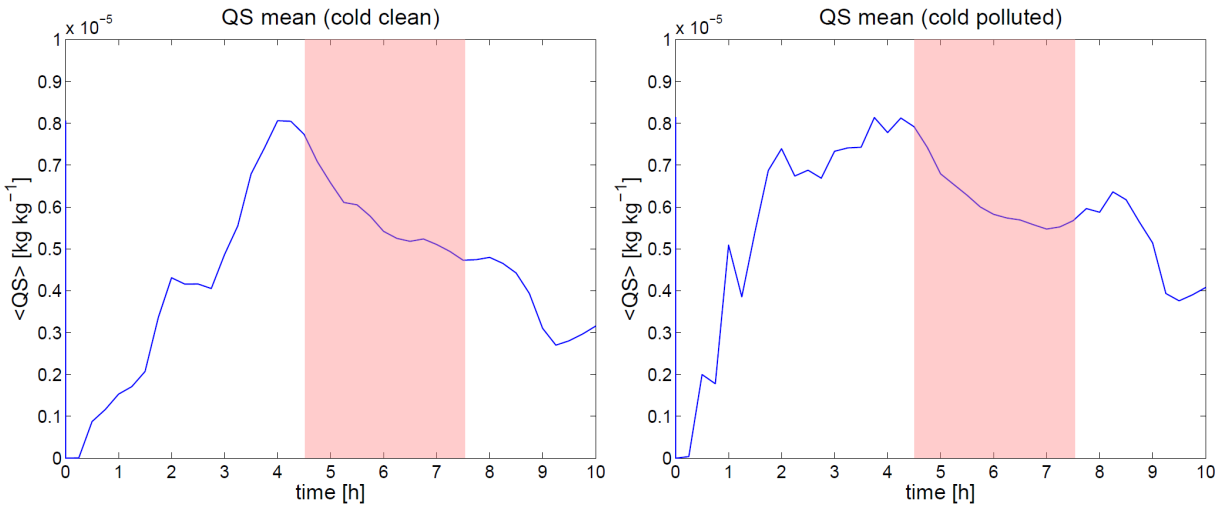

(a) (b)

Figure 4.1: **Integrated time average over the whole computational domain of snow**: The integrated time average over the whole computational domain of snow for the clean (left) and polluted (right) case is shown in this figure. The red area indicates the time period between t=4.5 h and t=7.5 h of the simulation over which the different variables are averaged.

4.2 Thresholds and analysis of computational domain

Since we want to examine susceptibilities of different microphysical processes in mixed-phase clouds, we first have to get an overview over the location of the clouds. For this purpose we regard the absolute values of different moisture variables. A lower threshold value is set for each quantity. These are described in table 4.1. These threshold values are maintained across the whole study.

Variable	Threshold
cloud droplet number concentration QNC	10^6 kg^{-1}
ice crystal number concentration QNI	10^3 kg^{-1}
mixing ratio of cloud water QC	10^{-7} kg kg^{-1}
mixing ratio of cloud ice QI	10^{-7} kg kg^{-1}
mixing ratio of rain QR	10^{-7} kg kg^{-1}
mixing ratio of snow QS	10^{-7} kg kg^{-1}
mixing ratio of graupel QG	10^{-7} kg kg^{-1}

Table 4.1: **Thresholds for the different moisture variables**

The cloud droplet (QNC) and ice crystal number concentration (QNI) for the clean and polluted case are shown in figure 4.2. QNC is restricted to an area between 400 and 450 km and a maximum altitude of 4000 m on the left side of the mountain.
On the contrary, QNI is also present on the right side of the mountain. There is a region

of high QNI around 470 km at heights between 5000 and 7000 m where QNI reaches values up to $4.6{\cdot}10^5\,\mathrm{kg}^{-1}$. One reason why there is no QNC in this region can be found in the vertical temperature profile (red lines). In these altitudes, temperature reaches values of -40 °C and lower. Pure water droplets in the atmosphere are known to supercool to about -38 °C before they freeze homogeneously [*Koop et al.*, 2000]. Thus, due to the onset of homogeneous freezing no liquid water droplets exist at these altitudes.
The shape of the potential temperature lines (grey) indicates the presence of a linear hydrostatic mountain wave (see *Muhlbauer et al.* [2010]).
The mixing ratios of cloud water (QC) and cloud ice (QI) show a similar pattern to that of QNC and QNI. The corresponding plots can be found in A.3.

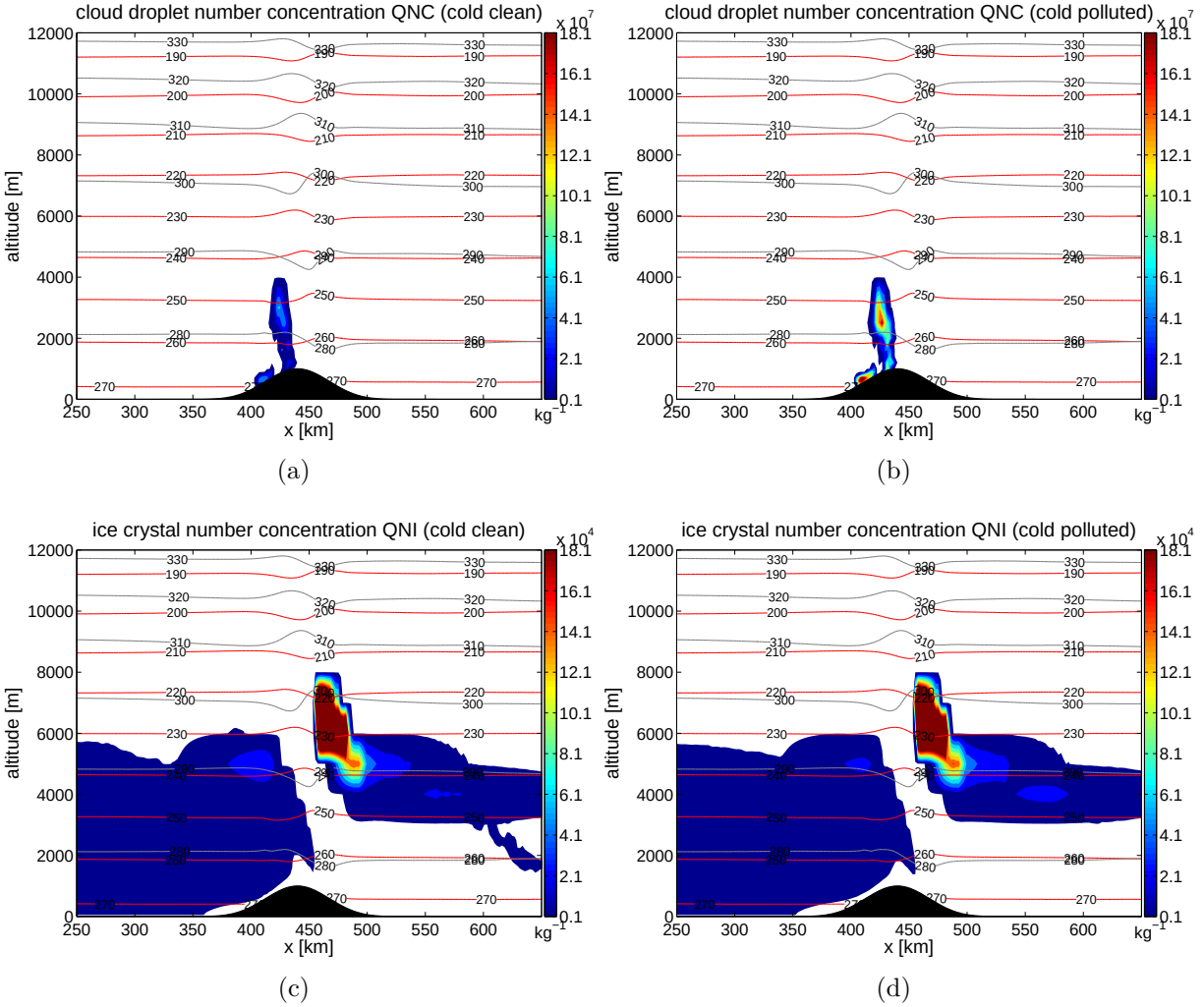

Figure 4.2: **Vertical cross section of QNC and QNI**: Vertical cross section of the number concentrations of cloud droplets (top) and ice crystals (bottom) averaged over t=4.5 h to t=7.5 h of SIM_cc (left) and SIM_cp (right). The contour lines indicate the temperature (red) and the potential temperature (grey).

From these observations, we can state that there is an orographic mixed-phase cloud on the upstream side of the mountain and an orographic ice-phase cloud on the leeward side of the mountain. The ice-cloud is formed by gravity waves. On the left edge of the domain there are some boundary effects which are not considered further.
Thus, the computational domain can be divided into different sectors which are displayed in table 4.2: from 250 to 420 km the 'border effect clouds', from 420 to 460 km the mixed-phase cloud and from 460 to 550 km the ice-phase cloud. In the following we are focusing on the mixed-phase cloud.

Cloud type	Sector
Boundary effect clouds	250-420 km
Orographic mixed-phase cloud	420-460 km
Orographic ice-phase cloud	460-550 km

Table 4.2: **Specification of the different sectors with the corresponding cloud type**

The mass mixing ratios of the various precipitation-size hydrometeor classes of SIM_cc and SIM_cp are shown in figure 4.3. We choose the same scale for the different hydometeors, in order to compare the absolute amount of precipitation between the three types of precipitation. SIM_cc and SIM_cp show mainly contributions from frozen hydrometeors (graupel and snow), whereas the contribution of rain is of smaller magnitudes.
Rain and graupel are restricted to the mixed-phase cloud, since they require the presence of liquid cloud droplets. On the other hand, a small amount of snow is also formed in the ice-phase cloud. However, snow is thought to evaporate before it reaches the ground which is indicated by the white area. The rain which is formed in the mixed-phase cloud does also not reach the ground as rain. According to figure 4.3(e) and 4.3(f) riming may occurs and thus, the initially formed rain reaches the ground as graupel. On the windward side of the mountain there is supposed to be a 'melting line' at an altitude of around 500 m (at a temperature around of 273 K) which is indicated by the presence of a narrow band of rain. When snow falls through this zone melting processes occurs and a part of the ice crystals melt producing rain. A small fraction of graupel is also formed.

Concluding we can say that we have different types of clouds and hydrometeor classes in our considered domain. In the following we are focusing on the microphysical processes in mixed-phase clouds. Thus, in contrast to warm-phase clouds it is important to consider also the frozen components.

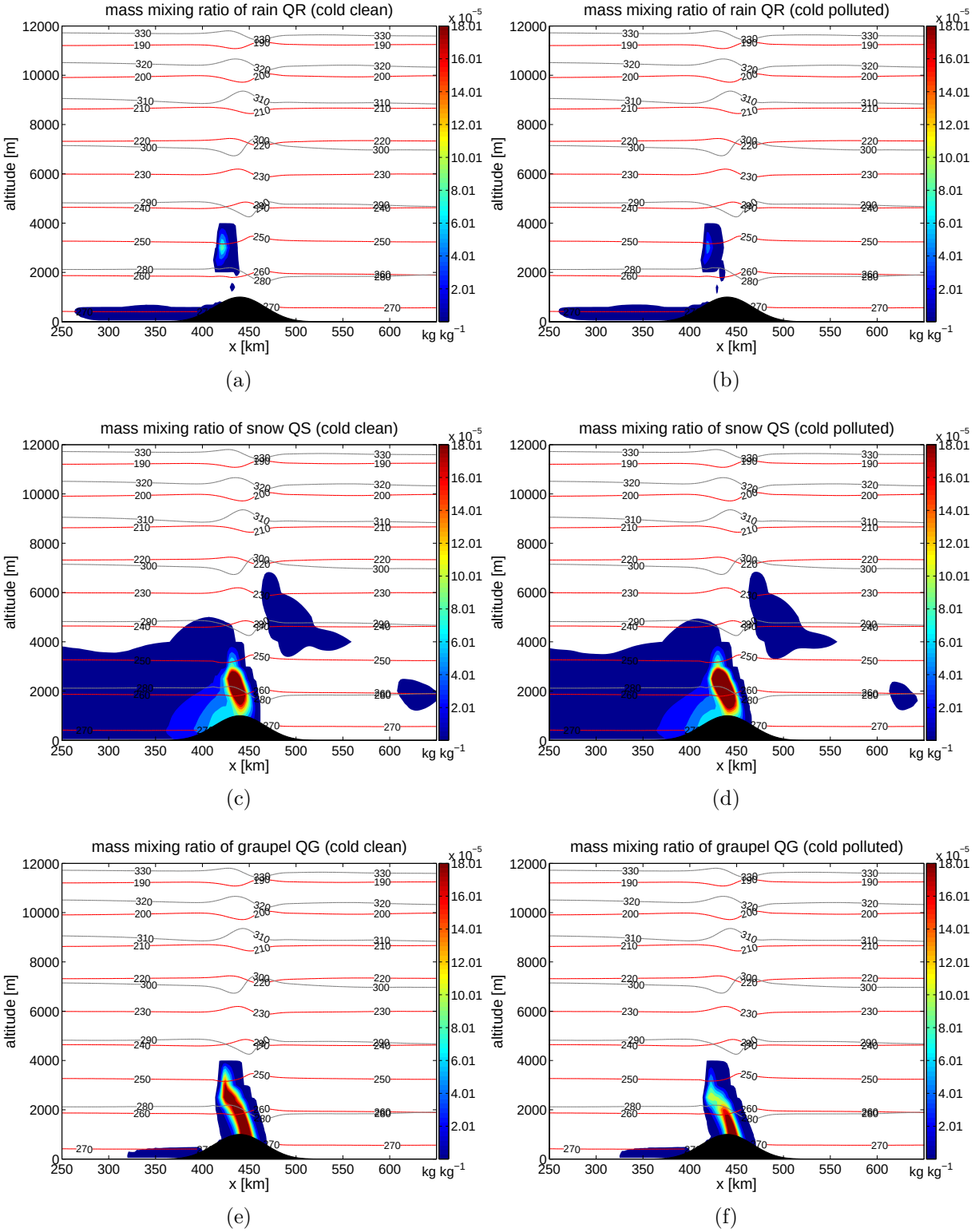

Figure 4.3: **Vertical cross section of QR, QS and QG**: Vertical cross section of the mass mixing ratios of rain (top), snow (middle) and graupel (bottom) averaged over t=4.5 h to t=7.5 h of SIM_cc (left) and SIM_cp (right). The contour lines indicate the temperature (red) and the potential temperature (grey).

4.3 From aerosols to cloud water/cloud ice

The first step of the IAE involves the link between aerosols and CCN/IN. However, both variables (CCN and IN) do not exists in our model output. We only have activation and freezing rates. *Herger* [2013] approximated the amount of CCN by the activation rate. Thus, we initially approximated the amount of CCN by the activation rate and the amount of IN by the freezing rate. The plots of the relative differences of the activation and freezing rates can be found in A.4. However, the activation rate and especially the freezing rate are problematic measures for CCN/IN because they strongly depend on supersaturation and temperature. Therefore, in this study the number of CCN (IN) is approximated by the mass of particles in the accumulation mixed mode (by the mass of black carbon (BC) and dust (DU) in the accumulation mixed mode). This implies that it is not possible to compute a value for the susceptibility of this step (aerosols to CCN/IN). Thus, we have combined the first and second step of the IAE, which includes now the link between aerosols and cloud water/cloud ice.

4.3.1 Susceptibilities of cloud water/cloud ice to aerosols

4.3.1.1 Evaluation

The relative differences of CCN and IN between the clean and polluted case are shown in figure 4.4. The red colour indicates that the CCN (IN) concentration is higher in the polluted case compared to the clean case. The relative difference is homogeneous over the whole domain for both CCN and IN.

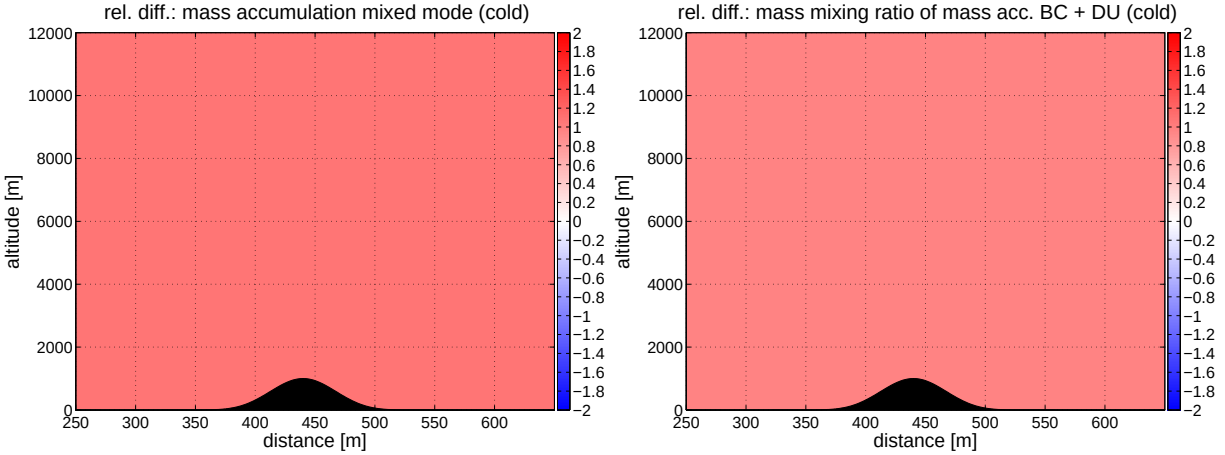

(a) (b)

Figure 4.4: **Relative differences of CCN and IN**: (a) relative difference of CCN, (b) relative difference of IN. CCN corresponds to the mass of particles in the accumulation mixed mode, while IN corresponds to the mass of black carbon and dust in the accumulation mixed mode.

The relative differences of cloud droplet (QNC) and ice crystal number concentrations (QNI) are shown in figure 4.5. According to figure 4.5(a), QNC is enhanced over the windward side of the mountain in the polluted case compared to the clean case. The relative difference of QNC is large over the mixed-phase cloud, with a geometric mean value of 0.94.
The relative difference of QNI is also positive over this region, with a geometric mean of 0.17, which is considerably lower than that of QNC. On the contrary, the sector between 350 and 410 km is mainly characterized by a blue area, which indicates that QNI is reduced in the polluted case compared to the clean case.
Both the relative differences of QNC and QNI are zero to the leeward side of the mountain.

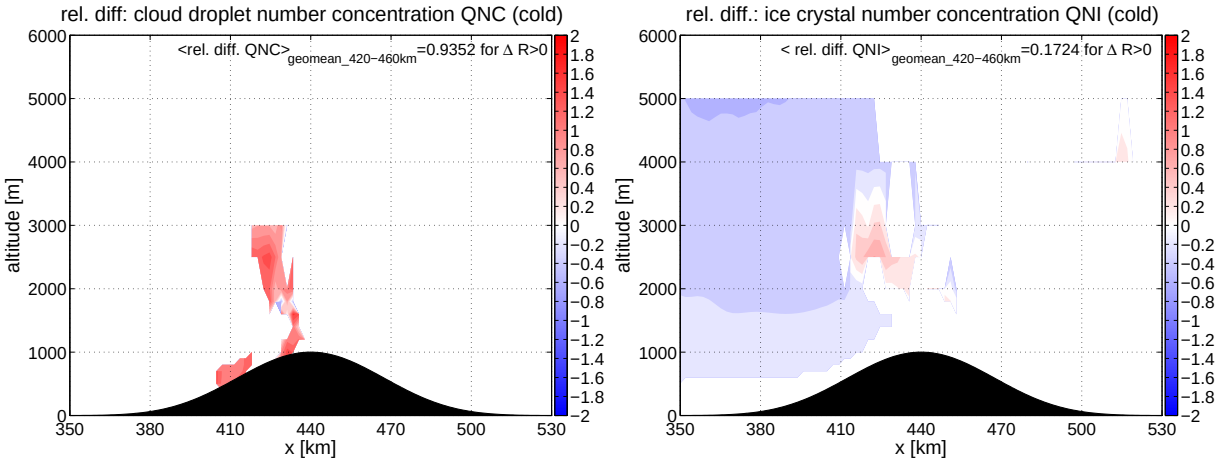

(a) (b)

Figure 4.5: **Relative differences of QNC and QNI**: (a) relative difference of QNC, (b) relative difference of QNI. The geometric mean of the relative differences is applied for the area within 420 and 460 km.

Since we now have examined the relative differences of the different variables between the polluted and the clean case, in a next step, we are interested in relating the changes in cloud water/cloud ice to changes in the aerosol abundance by calculating susceptibilities. This is done by using equation (3.3). For each point of the domain we compute a value for the susceptibility, which are then combined in order to determine the geometric mean of the susceptibility over a particular region. The susceptibilities of (a) the number concentration of cloud droplet (QNC) to the mass of particles in the accumulation mixed mode (m_acc) and (b) the number concentration of ice crystals (QNI) to changes in mass of BC and DU in the accumulation mixed mode (m_acc_BC_DU) are shown in figure 4.6. Since the susceptibilities of QNC to m_acc and of QNI to m_acc_BC_DU are basically the combination of figure 4.4 and 4.5, and as the relative differences of CCN and IN in figure 4.4 are homogeneous over the whole domain, the susceptibility plots in figure 4.6 look the same as the plots of the relative difference of QNC and QNI, respectively.

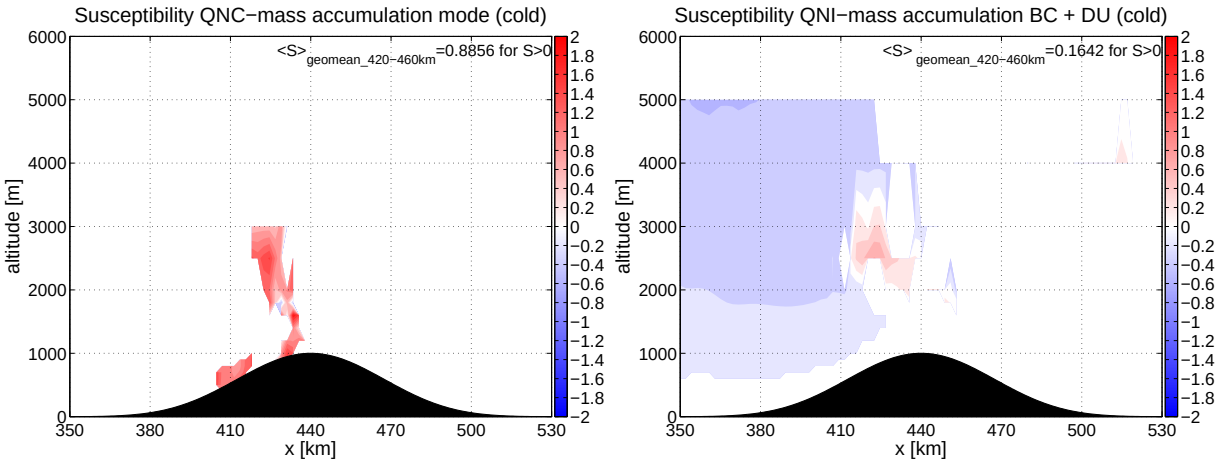

(a) (b)

Figure 4.6: **Susceptibilities of QNC to m_acc and of QNI to m_acc_BC_DU**: (a) Susceptibilities of QNC to changes in m_acc, (b) Susceptibilities of QNI to changes in m_acc_BC_DU. The geometric mean of the susceptibilities is applied for the area within 420 and 460 km.

Over the mixed-phase cloud, we retain mainly positive values for the susceptibility of QNC to changes in m_acc. The geometric mean over this region is around 0.9. The geometric mean of the susceptibility of QNI m_acc_BC_DU over the same area is 0.16.
Hence, over the mixed-phase cloud, the number concentration of ice crystal is less susceptible to changes in the aerosol abundance than the number concentration of cloud droplets.

4.3.1.2 Comparison to susceptibilities of the Jungfraujoch setup

In this section, we compare our susceptibilities to the values from the Jungfraujoch setup. In contrast to this study, *Herger* [2013] have calculated susceptibilities for both the first and the second step of the IAE. A value of approximately 1.2 is obtained for the susceptibility of CCN to the mass of the accumulation mixed mode (cf. figure 4.3(b) [*Herger*, 2013]), while the susceptibility of QNC to CCN is around 1 (cf. 4.5(a) [*Herger*, 2013]).
Since susceptibilities are multiplicative, it is possible to estimate the susceptibilities of combined steps along the IAE path. According to that, the susceptibility of QNC to changes in the aerosol abundance is given by the product of 1.2 and 1 which results in a value of 1.2. If we compare this number to the susceptibility of 0.9 which is recorded in our simulations along the same step, we find that the susceptibilities differ. We assume that one reason for this discrepancy can be found in the different aerosol dynamics and activation parameterisations within the two setups.

For the link between QNI and the mass of BC and DU in the accumulation mixed mode we cannot find any literature to compare our values. However, in general it can be said that QNI is less susceptible to changes in the aerosol concentration compared to QNC.

4.4 From cloud water/cloud ice to precipitation

The final step of the IAE includes the link between cloud water/cloud ice and precipitation. In contrast to warm-phase clouds, precipitation in mixed-phase clouds is not restricted to the liquid phase. Thus, as we have seen in section 4.2, frozen components like snow and graupel which are summarised under the term frozen precipitation need to be taken into account.
The following variables are considered along this path: cloud water (QC) and cloud ice content (QI), number concentrations of cloud droplets (QNC) and ice crystals (QNI) and mixing ratios of rain (QR) and frozen precipitation (QF). The relative differences of these variables are displayed in figure 4.7.

In the following, we will first focus on the link between cloud water and rain, while the step from cloud water/cloud ice to frozen precipitation is discussed afterwards. Before we compute values for the susceptibilities of this step, we will examine the IAE in mixed-phase clouds by looking at the relative differences of different hydrometeor variables.

4.4.1 Analysis of the IAE of warm-phase processes

The relative differences of the cloud droplet number concentration (QNC) and of the mass mixing ratios of cloud water (QC) and rain (QR) are shown in figure 4.7 (left part). By combining 4.7(a), 4.7(c) and 4.7(e) we can try to visualize the IAE on warm-phase processes in mixed-phase clouds: The number of cloud droplets is increased in the polluted case compared to the clean case over the entire height of the mixed-phase cloud (cf. 4.7(e)). In contrast, a reduction of rain is only observed in the upper part of the mixed-phase cloud at an altitude between 2500 and 3000 m (cf. 4.7(a)). By comparing this region of reduced rain formation to the plot of the relative difference of cloud water (cf. 4.7(c)), it is striking that this region complies with the area in which QC is reduced in the polluted case indicated by the blue colour. Thus, since in the polluted case QC is reduced and distributed over an increased number of droplets, there are more but smaller cloud droplets in the upper part of the mixed-phase cloud.
The cloud droplets are assumed to be spherical in shape and to have the same size. Using this approach we calculate the mean radius of the droplets by dividing QC by QNC. We compute that on average the radius of the cloud droplets is approximately 20 % lower in the polluted case compared to the clean case within the section between 420 and 460 km. According to *Twomey* [1977], this shift in the cloud droplet size distribution toward smaller sizes reduces the collision-coalescence efficiency and thus leads to suppression of rain.
Thus, we can state that the IAE related to the warm-phase microphysical processes is pronounced in the upper part of the mixed-phase cloud.

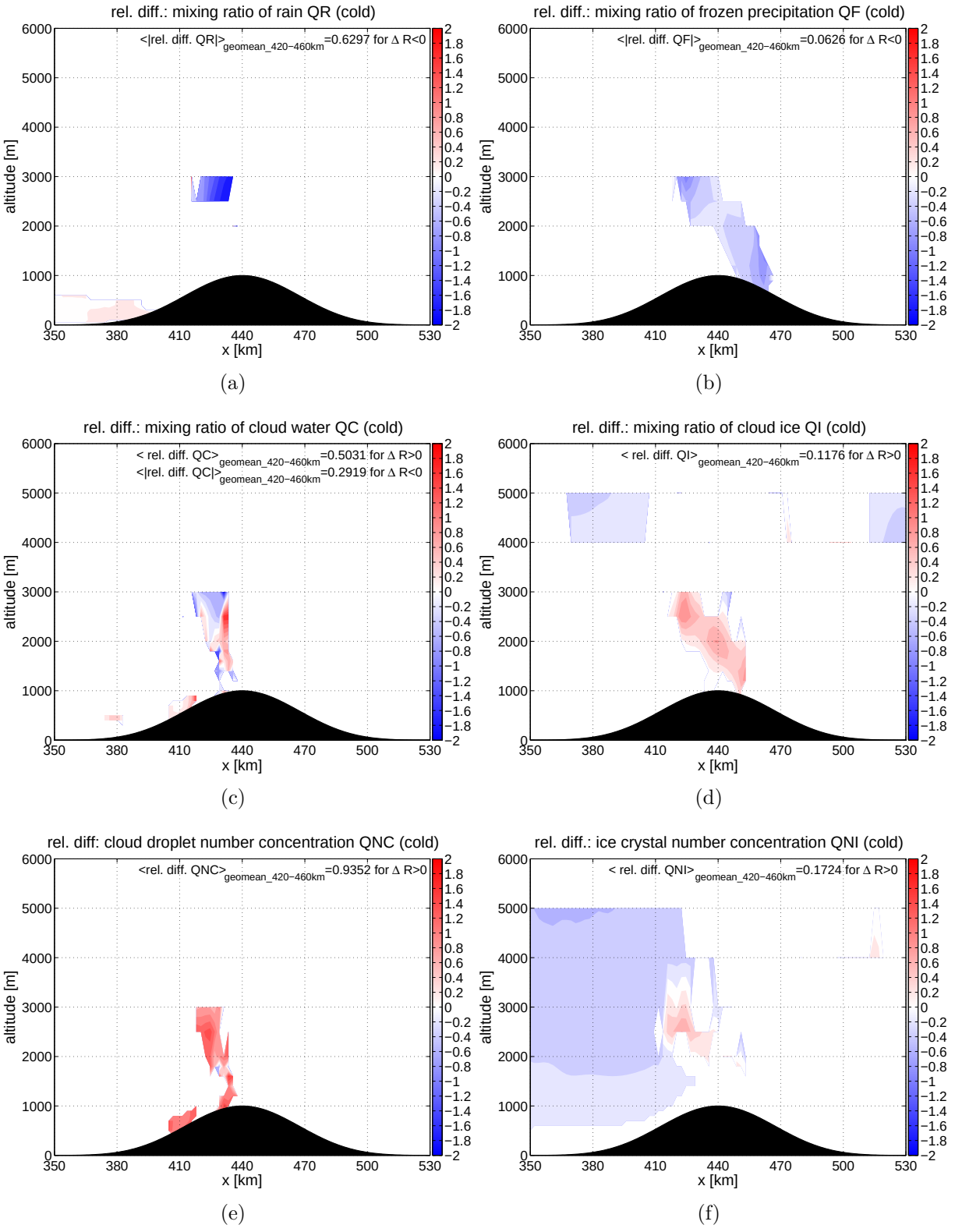

Figure 4.7: **Relative differences of QR, QF, QC, QI, QNC and QNI**: relative difference of (a) QR, (b) QF, (c) QC, (d) QI, (e) QNC, (f) QNI. The geometric mean of the relative differences is applied for the area within 420 and 460 km.

4.4.2 Analysis of the glaciation indirect effect

As we have been able to observe the IAE on warm-phase processes in mixed-phase clouds by combining the different plots of the relative differences, the question arises whether it is possible to observe the glaciation indirect effect using the same method. For this purpose we compare 4.7(b), 4.7(d) and 4.7(f): A positive relative difference of QNI is recorded over the mixed-phase cloud (cf. 4.7(f)). QI is also increased in the polluted case in comparison to the clean case over this region (cf. 4.7(d)). On the basis of augmented QNI and QI in the polluted case over the mixed-phase cloud and in accordance to the glaciation indirect effect described in section 2.1, we would expect an increase of frozen precipitation. However, a reduction of frozen precipitation over the entire mixed-phase cloud is shown in figure 4.7(b). It needs to be pointed out however, that the relative difference of frozen precipitation between the clean and the polluted case is small. A geometric mean of around 0.06 is computed for the relative difference of QF over the mixed-phase cloud. Thus, we can say that there is no substantial change in QF.

Now the question arises why we could not observe an increase in QF as we would expect. As mentioned before, frozen precipitation consists of snow and graupel. In the following, we consider the components of frozen precipitation separately. Figure 4.8 shows the relative differences of the mixing ratios of snow (QS) and graupel (QG).

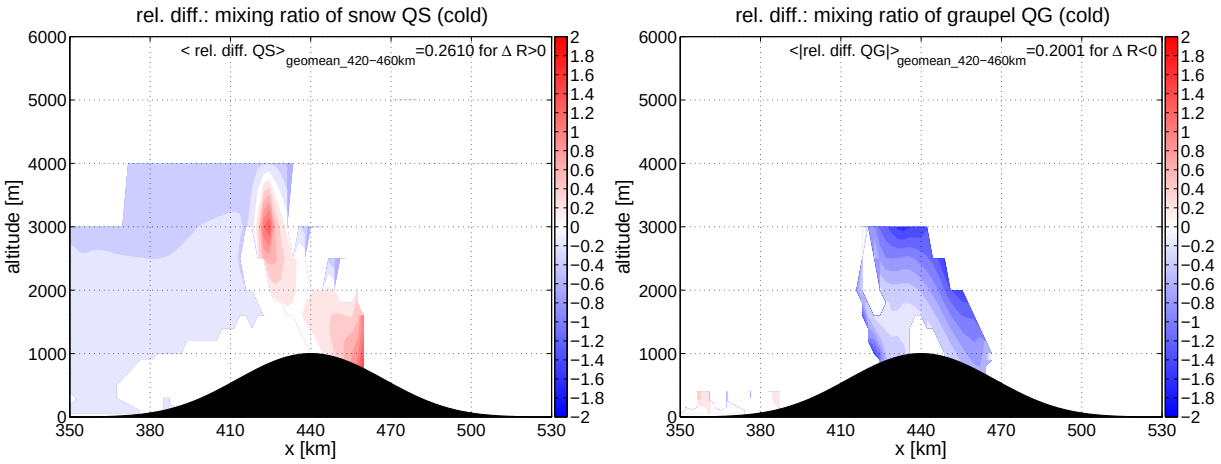

(a) (b)

Figure 4.8: **Relative differences of QS and QG**: (a) relative difference of QS, (b) relative difference of QG. The geometric mean of the relative differences is applied for the area within 420 and 460 km.

Over the mixed-phase cloud, positive values are recorded for the relative difference of QS. This would lead to an increase in frozen precipitation in the polluted case. However, by regarding the second component, namely graupel, we observe an opposite effect. For the relative difference of QG we obtain negative values over the mixed-phase cloud. This means that we have a reduction of graupel in the polluted case compared to the clean case.

We propose that one reason for the reduction in graupel is the reduced riming efficiency in the polluted case which results from the shift in the cloud droplet size distribution towards smaller sizes. As mentioned above, on average, we determine a reduction of 20 % in the cloud droplet radius in the polluted case as compared to the clean case over the mixed-phase cloud. This hypothesis of a reduced riming efficiency is supported by a study of *Borys et al.* [2000] which states that the riming efficiency declines for droplets with smaller diameters.
On the other hand, the increase in QS may could be partially explained by the change in the ice crystal mass between the polluted and the clean case. We compute an average increase of 25 % in the ice crystal mass in the polluted case over the mixed-phase cloud. This would enhance the Bergeron-Findeisen process and thus explain the increase in QS. Furthermore, according to the graupel formation parametrisation equation from *Seifert and Beheng* [2006] which is used in the simulations, this increase in the ice crystal mass leads to a further reduction in the graupel formation rate in addition to the reduction caused by the smaller cloud droplet diameters.

Thus, the slight decrease in QF (cf. 4.7(b)) in the polluted case relative to the clean case may partially be explained by the fact that the decline in cloud droplets radius (which results in a reduced riming efficiency) could not be fully compensated by the increase in the ice crystal mass (which leads to an increased Bergeron-Findeisen process). Therefore, a slight suppression in frozen precipitation is detected and the glaciation indirect effect described in section 2.1 could not be observed.

4.4.3 Susceptibilities of rain to cloud water

After having analysed relative differences of these different moisture variables and having visualized the IAE in mixed-phase clouds, in the following, the relation of these variables is examined by determining values for susceptibilities. We will first discuss the warm-phase microphysical processes.

4.4.3.1 Evaluation

Figure 4.9 shows the susceptibility of rain (QR) to changes in the cloud droplet number concentration (QNC). We record negative susceptibilities over the mixed-phase cloud, with a geometric mean of -0.65. The negative sign indicates that QR and QNC are negatively correlated, i.e. a suppression of rain is observed in the case of an increase in QNC. According to equation (3.3) the difference of QR between the polluted and the clean case is smaller than the relative difference of QNC, since we record a value below 1 for the susceptibility.

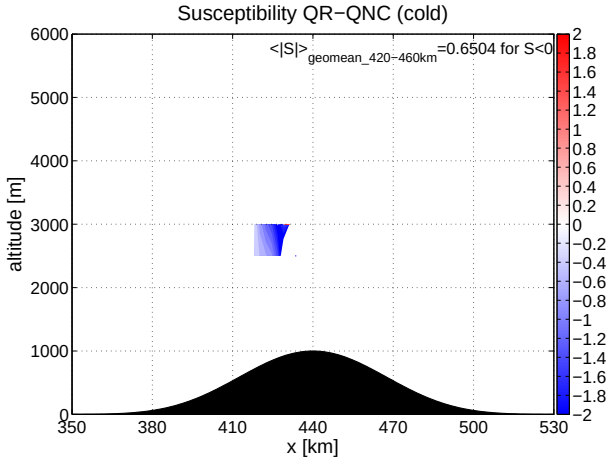

Figure 4.9: **Susceptibility of QR to QC**: Susceptibility of QR to changes in QNC. The geometric mean of the susceptibility is applied for the area within 420 and 460 km.

4.4.3.2 Comparison to the Jungfraujoch setup and to literature values

In the following, we want to compare this susceptibility value for the link between QR and QNC to other studies in order to verify the plausibility of the result.
By comparing this mean value of -0.65 to the susceptibility of QR to QNC determined by *Herger* [2013] it can be noticed that the values are similar. *Herger* [2013] reports a susceptibility of around -0.6 for the link between QR and QNC (cf. figure 4.9(b) [*Herger*, 2013]).
In addition, this value is also located in the susceptibility value range for low liquid water path (LWP) proposed by *Sorooshian et al.* [2009]. In their paper they report that the precipitation susceptibility is a non-monotonic function of LWP. According to that function it can be differentiated between three regimes depending on the LWP (cf. 4.10). Since in our study the simulations are run for cold temperatures, QC and thus LWP is low. Hence, we focus primarily on the low-LWP regime. As shown in figure 4.10, the precipitation susceptibilities in this regime (blue area) are between 0.6 and 0.7. It has to be considered that in contrast to our study *Sorooshian et al.* [2009] have chosen a negative sign for the definition of the precipitation susceptibility. Therefore, we have to compare the absolute values. If we compare our mean susceptibility of -0.65 to this susceptibility range it is apparent that our obtained value fits in well into this regime.

4.4.4 Susceptibilities of frozen precipitation to cloud water/ice

In the following, we discuss the susceptibilities of frozen precipitation. Since there exist different microphysical processes which leads to the formation of frozen precipitation involving both cloud water and cloud ice, we calculated the susceptibilities of QF to cloud water as well as the susceptibilities of QF to cloud ice.

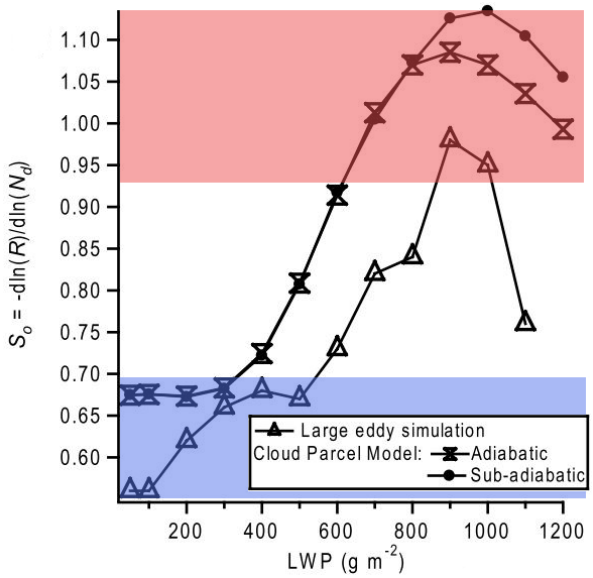

Figure 4.10: **Precipitation susceptibility as a function of LWP**: The blue area corresponds to the regime with low LWP and low susceptibilities. Adapted from [*Sorooshian et al.*, 2009].

4.4.4.1 Evaluation

Figure 4.11 shows the susceptibilities of QF to QNC, QC, QNI and QI.
For the susceptibility of QF to QC we find mainly positive values over the mixed-phase cloud. The geometric mean of the susceptibility over this area is 0.50. On the contrary, slightly negative values are recorded for the susceptibility of QF to QNC over the same area, with a geometric mean value of –0.06. Note that the susceptibilities of QF to cloud water are observed only over a limited area of the mixed-phase cloud.
For the susceptibility of QF to QNI we denote mostly negative values over the mixed-phase cloud, with a geometric mean of -1.0. The susceptibility of QF to QI is also characterised through mainly negative values. The geometric mean of the susceptibility of QF to QI assumes a value of -0.32.
If we compare these susceptibilities of QF (cf. 4.11) to the susceptibility of QR to QNC (cf. 4.9), it is remarkable that in general frozen precipitation is less susceptible to changes in the initial aerosol concentration than rain. Only for the link between QF and QNI we record higher susceptibilities compared to the value of -0.65 for the link between QR and QNC. This relative high value of -1.0 for the geometric mean of the susceptibility of QF to QNI may could be explained by the fact that it may is influenced by artefacts. We suppose that this value contains the largest error and thus is associated with the largest uncertainty.

In the subsequent section, we want to evaluate whether this hypothesis of a reduced susceptibility for ice-phase processes can be supported by theory.

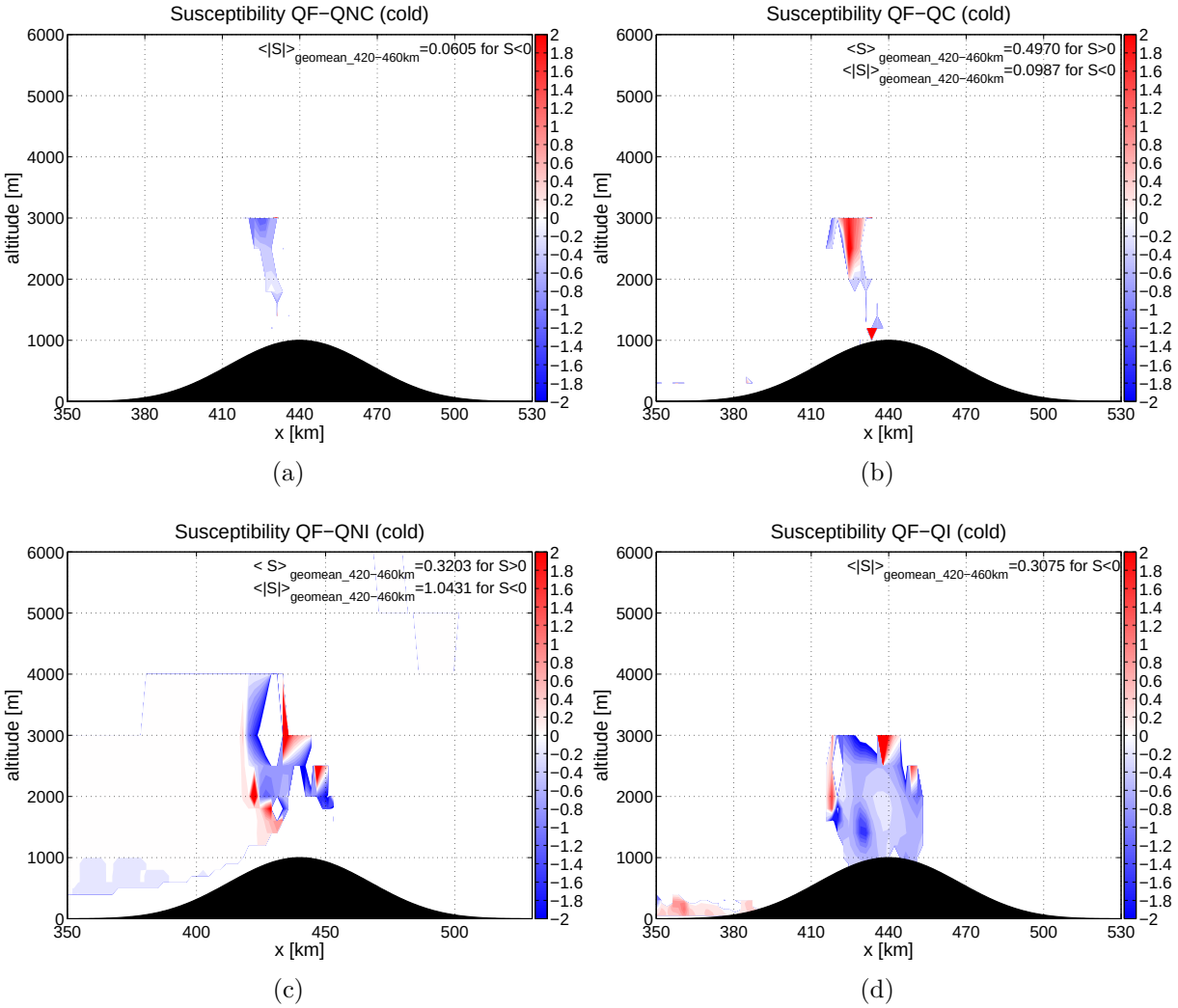

Figure 4.11: **Susceptibilities of QF to QNC, QC, QNI and QI**: (a) Susceptibility of QF to changes in QNC, (b) Susceptibility of QF to changes in QC, (c) Susceptibility of QF to changes in QNI, (d) Susceptibility of QF to changes in QI. The geometric mean of the susceptibilities is applied for the area within 420 and 460 km.

4.4.4.2 Comparison to a semi-theoretical value

Since *Herger* [2013] has focused on warm-phase processes and no literature is available to compare the susceptibilities of frozen precipitation, we calculate a semi-theoretical value in order to examine the extent to which the obtained values in the previous section are reliable.

Seifert and Beheng [2006] (eq. 61 + 78) parametrise the mass transfer in cold-phase collection processes by

$$\begin{aligned}\left.\frac{\partial L_a}{\partial t}\right|_{\text{collection}} &\propto [c_1 D_a^2 + c_2 D_a D_b + c_3 D_b^2][c_4 D_a^{2\beta_a} - c_5 D_a^{\beta_a} D_b^{\beta_b} + c_6 D_b^{2\beta_b} + c_7]^{0.5} \\ &=: Q(N_a, L_b, D_a(N_a, L_a), D_b(N_b, L_b))\end{aligned} \tag{4.1}$$

where the index a (b) denotes the collecting (collected) hydrometeor species, L_x (N_x) the mass (number) densities and D_x the hydrometeor diameter. The values for β_c are given by *Seifert and Beheng* [2006] (Tab. 1) and the constants c_1 to c_7 are positive and have similar orders of magnitude.

Due to the change in pathway for frozen precipitation formation from riming and graupel to aggregation and snow, it is hard to choose a single function for the susceptibility analysis, which then corresponds to the autoconversion studied in the warm case.

One sensible choice seems the riming of ice crystals i by cloud droplets c,

$$i + c \rightarrow \begin{cases} i \\ g \end{cases}$$

which may result in ice i or graupel g. This process thus takes place before the split of pathways.
It can be assumed that the collecting and the collected particle have about the same size and thus the same fall speed, i.e.

$$D_a \approx D_b \approx D_a^{0.5} D_b^{0.5}$$

where the geometric mean is chosen to keep the further calculation convenient. For the exponents the geometric mean can be applied as well:

$$\beta := \sqrt{\beta_a \beta_b} \approx \beta_a \approx \beta_b$$

These assumptions reduce (4.1) to

$$\begin{aligned} Q &\propto N_a L_b D_a D_b D_a^{\frac{\beta}{2}} D_b^{\frac{\beta}{2}} \\ &= N_a L_b D_a^{\frac{2+\beta}{2}} D_b^{\frac{2+\beta}{2}} \end{aligned} \tag{4.2}$$

when c_7 is neglected. Inserting

$$D \propto \left(\frac{L}{N}\right)^{\frac{1}{3}}$$

yields

$$\begin{aligned} Q &\propto N_a L_b \left(\frac{L_a}{N_a}\right)^{\frac{2+\beta}{6}} \left(\frac{L_b}{N_b}\right)^{\frac{2+\beta}{6}} \\ &= L_a^{\frac{1}{3}+\frac{\beta}{6}} N_a^{\frac{2}{3}-\frac{\beta}{6}} L_b^{\frac{4}{3}+\frac{\beta}{6}} N_b^{-(\frac{1}{3}+\frac{\beta}{6})} \end{aligned} \tag{4.3}$$

and thus

$$Q \propto L_i^{0.4} N_i^{0.6} L_c^{1.4} N_c^{-0.4} \tag{4.4}$$

Comparing (4.4) to the autoconversion rate

$$\frac{\partial L_c}{\partial t} \propto L_c^4 N_c^{-2} \tag{4.5}$$

offers the interpretation that the ice-phase processes are generally less susceptible than the warm-phase processes. This would support the hypothesis we have proposed in the previous section.

Additionally, equation (4.4) can be probed by the simulation results. For that purpose we will compare the susceptibility of QF to QI to a semi-theoretical value for the same link using the following equations:

$$d\ln(QS+QG) = 0.4\, d\ln QI + 0.6\, d\ln QNI + 1.4\, d\ln QC - 0.4\, d\ln QNC$$

$$\begin{aligned} \Rightarrow \left\langle \frac{d\ln QF(x,h)}{d\ln QI(x,h)} \right\rangle = \\ 0.4 + 0.6 \left\langle \frac{d\ln QNI(x,h)}{d\ln QI(x,h)} \right\rangle + 1.4 \left\langle \frac{d\ln QC(x,h)}{d\ln QI(x,h)} \right\rangle - 0.4 \left\langle \frac{d\ln QNC(x,h)}{dlnQI(x,h)} \right\rangle \end{aligned} \tag{4.6}$$

For this, we first have to find an adequate area for which this calculation can be conducted. The first criterion that is applied is that all variables in the considered area (QC, QNC, QI, QNI, QF) have to be above the threshold values which have been defined in section 4.2. In addition, the values for the different susceptibilities (QF-QI, QNI-QI, QC-QI, QNC-QI) must have an uniformly distribution within the regarded area (i.e. no mixing of positive and negative values), so that a geometric mean over the considered region can be computed.
Figure 4.12 summarises the different susceptibilities which enter in equation 4.6. By comparing these different plots in figure 4.12, we can find an appropriate area. Between 425 and 431 km and at an altitude of around 2500 m there is a region which fulfils the above mentioned criteria. Hence, the calculation is conducted over this area in the upper part of the mixed-phase cloud.
Over this particular region, we compute a geometric mean of -0.41 for the susceptibility of QF to QI from the simulations. It can be noticed that it is slightly higher than the value we determined in the previous section over the entire mixed-phase cloud. By inserting the

geometric means of the susceptibilities of QNI-QI, QC-QI and QNC-QI in equation 4.6 we can calculate a semi-theoretical value for the susceptibility of QF to changes in QI:

$$\left\langle \frac{d \ln QF}{d \ln QI} \right\rangle = 0.4 + 0.6 \cdot 0.74 + 1.4 \cdot (-0.23) - 0.4 \cdot 1.7 = -0.16 \tag{4.7}$$

We determine a semi-theoretical value of -0.16 for the susceptibility of QF to QI. If we compare this value to the geometric mean of around -0.4 which is computed from the simulations, it is apparent that they differ. One reason for this discrepancy could be that some assumptions made in the course of the simplification of the parameterisation of the mass transfer in cold-phase collection processes are not justified.
A further point which has to be considered is that the calculation of the semi-theoretical value has been conducted over a small number of grid points, since there is a limited area over which the susceptibilities are distributed uniformly.

The calculation of the semi-theoretical value and its comparison to the susceptibility computed from the simulations gives us an idea of the error. We see that it is not reasonable to indicate the geometric mean of susceptibilities with more than two decimal places.

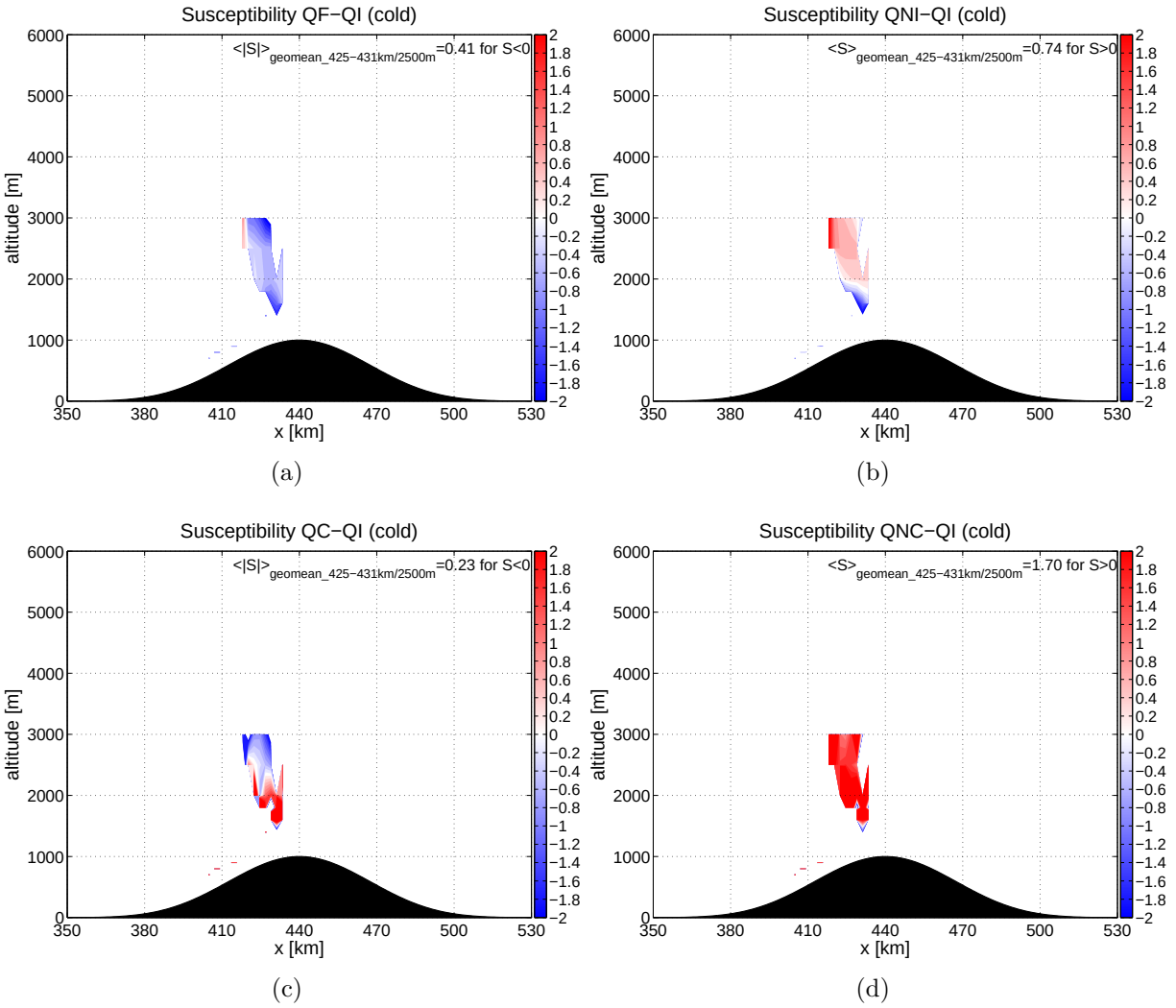

Figure 4.12: **Susceptibilities of QF-QI, QNI-QI, QC-QI and QNC-QI**: (a) Susceptibilities of QF to changes in QI, (b) Susceptibilities of QNI to changes in QI, (c) Susceptibilities of QC to changes in QI, (d) Susceptibilities of QNC to changes in QI. Susceptibilities are calculated only if all hydrometeor variables are above the corresponding threshold defined in section 4.2 (note that the shape of the contour plot is the same in all plots). The geometric mean of the susceptibilities is applied for the area within 425 and 431 km at an altitude of 2500 m.

Chapter 5

Conclusion

In the course of this study we have investigated the aerosol-cloud-precipitation interactions in mixed-phase clouds from a susceptibility perspective. We computed values for the susceptibilities for each step of the indirect aerosol effect. An overview of the different susceptibilities is given in table 5.1.

Susceptibility	Range	Simulation	Comparison
QNC-m_acc	420-460 km	0.9	1.2 (*Herger* [2013])
QNI-m_acc_BC_DU	420-460 km	0.2	
QR-QNC	420-460 km	-0.7	-0.6 (*Herger* [2013]) -0.6 to -0.7 (*Sorooshian et al.* [2009])
QF-QNC	420-460 km	-0.1	
QF-QC	420-460 km	0.5	
QF-QNI	420-460 km	-1.0	
QF-QI	420-460 km	-0.3	
	425-431 km/2500 m	-0.4	-0.2 (semi-theoretical value)

Table 5.1: **Summary of susceptibilities of warm- and cold-phase processes**

For the susceptibilities of the warm-phase processes we obtain values similar to the literature, which supports our approach of calculating susceptibilities. However, there is no literature available to compare the susceptibilities of the cold-phase processes so far. Thus, further studies have to been performed in order to analyse the susceptibilities of the cold-phase processes and consolidate the results reported here.

Comparing table 5.1 to the results of *Herger* [2013] it can be concluded that in general the susceptibilities of the cold-phase processes are lower compared to the warm-phase processes, i.e. cold-phase processes are less susceptible to changes in the initial aerosol concentration. This coincides with the results of *Muhlbauer et al.* [2010] where a lower aerosol signal was found in precipitation for the cases with low temperatures. In addition, the susceptibility values for the warm-phase processes are consistent with the results from

Herger [2013] despite the fact that we have used another model setup. This independence from the chosen setup is one advantage of the susceptibility concept, provided that values obtained at similar resolutions are compared [*McComiskey and Feingold*, 2012].

This study is associated with some limitations. The model setup does not implement all processes like for example aerosol-radiation interactions. The consideration of more processes is fundamental in order to increase the accuracy of the results. A further point which has to be considered it that we used a two dimensional setup and only analysed a single meteorological situation.
One major problem which came across and which has to be critically reflected on is the output of the simulations. We observed some strange boundary effects which proceeded through the computational domain and thus influenced the model output. Hence, we were not able to determine a steady-state since some moisture variables have not reached a constant value within the simulation time of 10 hours. For further studies we would strongly recommend to perform new simulations.

We conclude that in the course of this thesis we have seen that cold-phase processes are very complex in comparison to warm-phase processes. The estimation of these aerosol-cloud interactions remains one of the major challenges regarding the quantification of climate feedbacks and sensitivity. The performance of further studies is important in order to increase the understanding and quantification of cloud feedbacks and thus of the Earth's climate system.

Chapter 6

Acknowledgment

Writing this Bachelor thesis was only possible with the contribution and support of many people. At this point I would like to thank the following people for their engagement and involvement in the creation of this Bachelor thesis.

First of all, I would like to thank my supervisor Franziska Glaßmeier for her time, competent support and advices during the construction of this thesis. I have learned a lot throughout the entire working process. Thank you also for preparing the simulations.

Furthermore, I would like to thank Prof. Dr. Ulrike Lohmann for giving me the opportunity to write my Bachelor thesis in the Atmospheric Physics research group and providing me an insight into this field of study. Thank you also for your expertise during the various discussions in the course of this thesis.

I would also like to thank David Neubauer for his supervise during the time when Franziska Glaßmeier was absent. Thank you!

Thank you, Yvonne Boose and Jan Henneberger, for answering my questions regarding MATLAB!

I would also like to thank Nadja Herger for providing me her Bachelor thesis, for answering my questions and for proofreading my Bachelor thesis. Thank you!

Finally, I want to thank my family and friends for their support and encouragement throughout the writing of my Bachelor thesis.

Appendix A

Appendix

A.1 Atmospheric dynamical parameters

Figure A.1 shows the time evolution of water vapour (QV), horizontal (U) and vertical wind velocities. The left column shows the maximum values of QV, U and W. Domain averages of QV, U and W are displayed on the right column.

Figure A.2 shows the cross section of QV, U and W averaged over t=4.5 h to t=7.5 h of SIM_cc (left column). The relative differences of QV, U and W between the clean and polluted case are found on the right-hand side.

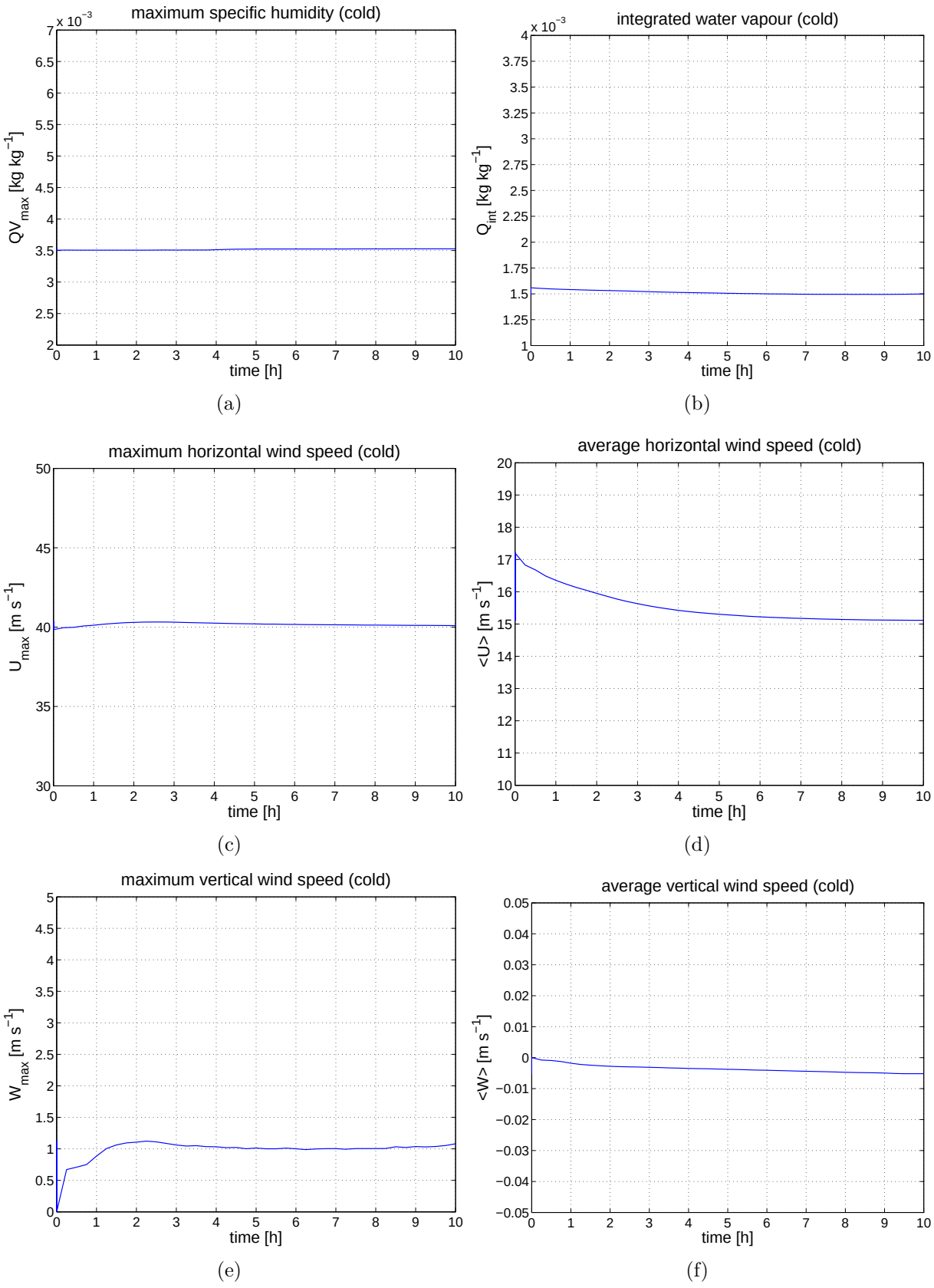

Figure A.1: **Time evolution of QV, U, W**

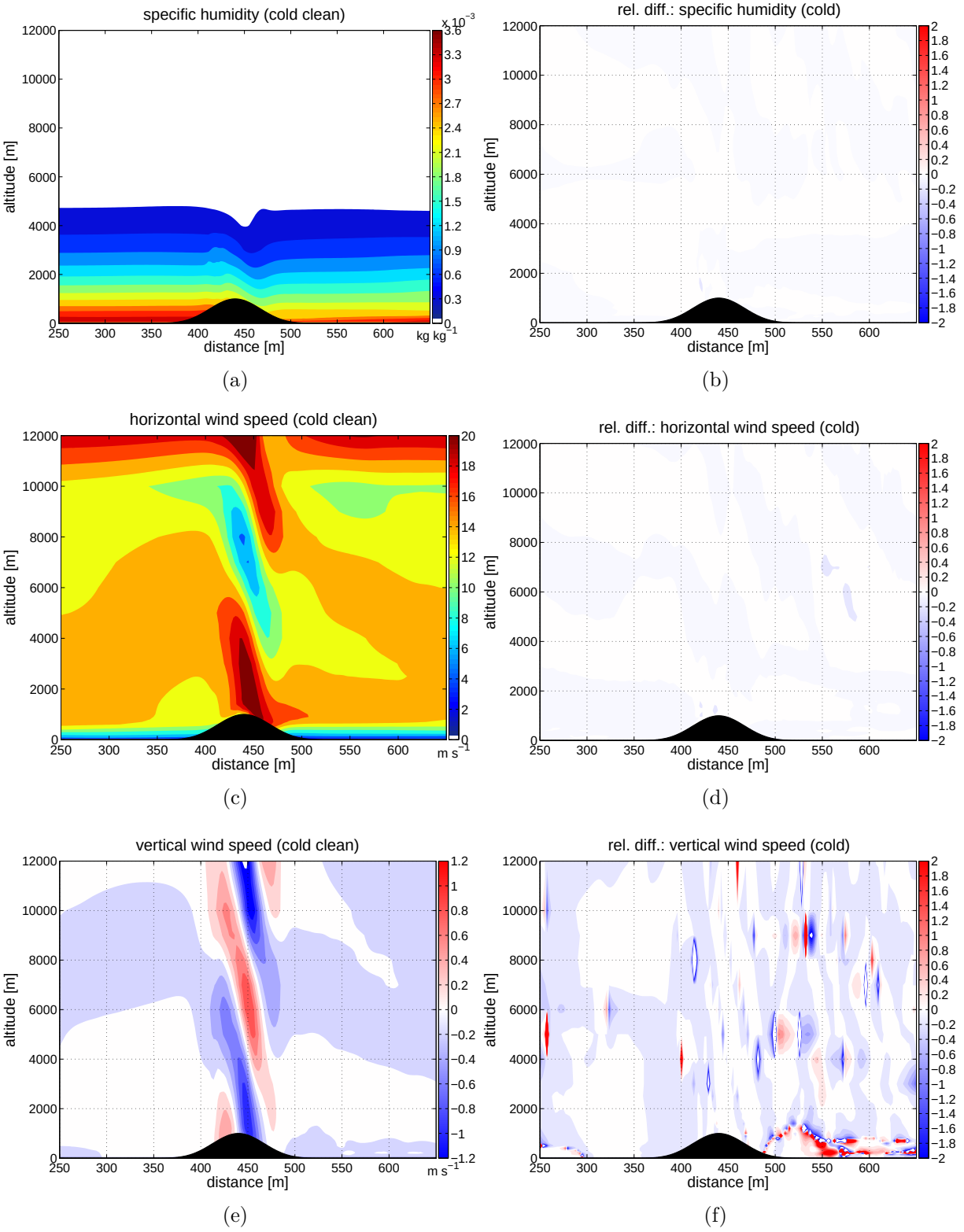

Figure A.2: **Vertical cross section and relative differences of QV, U and W**

A.2 Integrated time averages

In order to determine the time period over which the different variables are averaged, we have to identify a period which is comparable to a steady-state situation. For that purpose the integrated time averages of different hydrometeors are considered.
Figure A.3 shows the integrated time average over the whole computational domain of cloud droplet and ice crystal number concentration for the clean (left) and polluted (case). The integrated time average of the mass mixing ratios of cloud water and cloud ice are displayed in figure A.4, while the integrated time average of rain and graupel can be found in figure A.5.

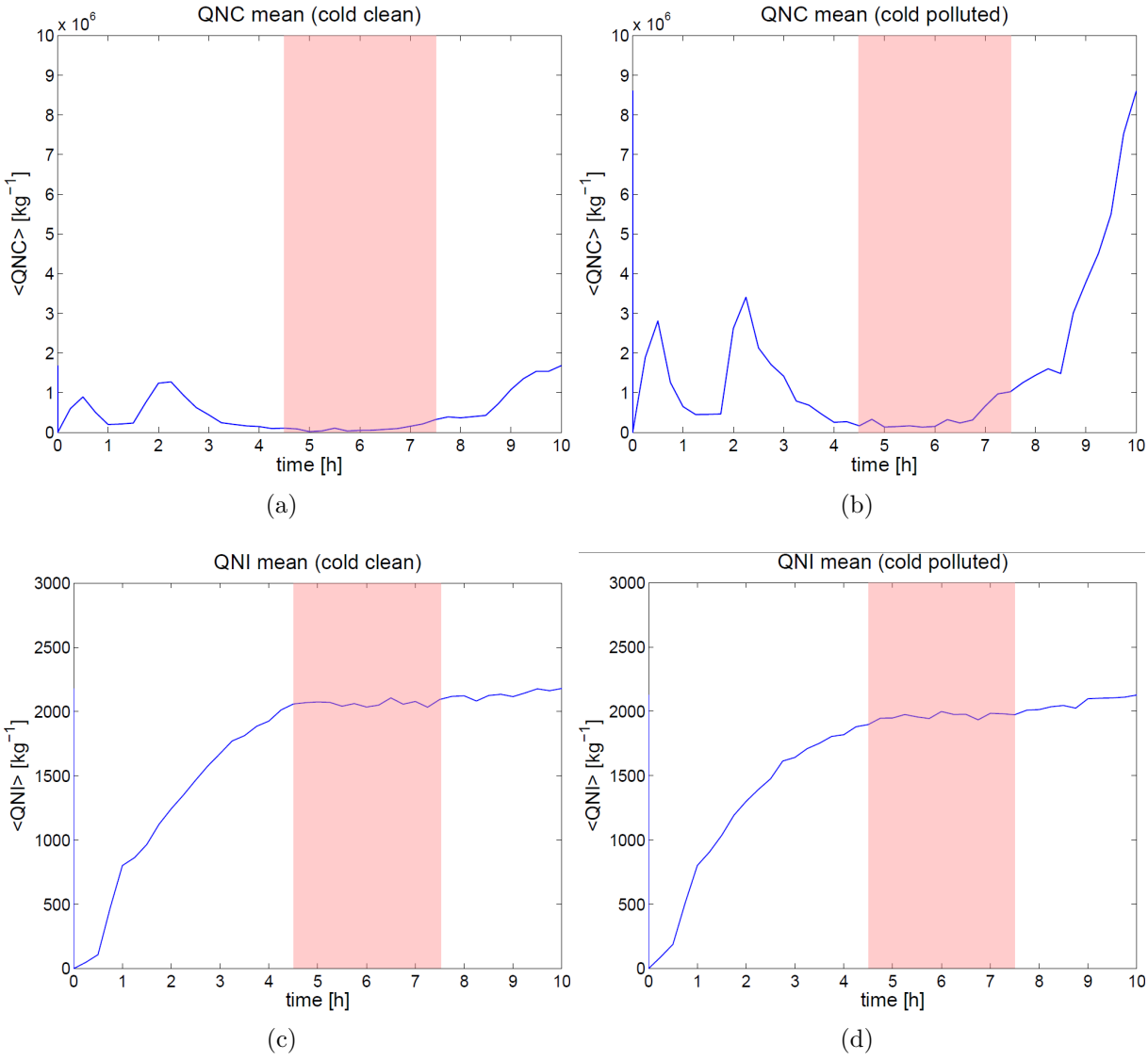

Figure A.3: **Integrated time averages of QNC and QNI**

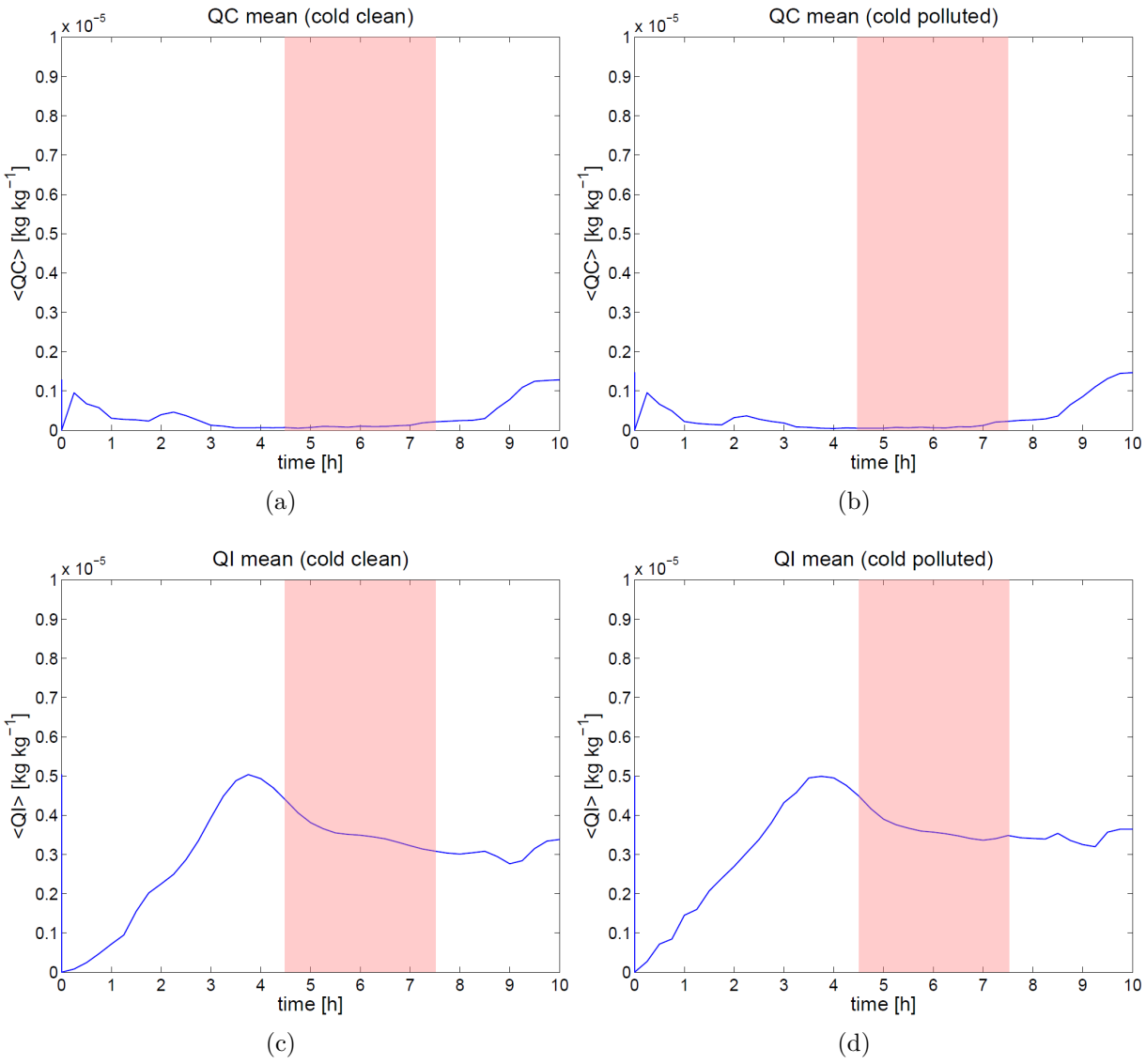

Figure A.4: **Integrated time averages of QC and QI**

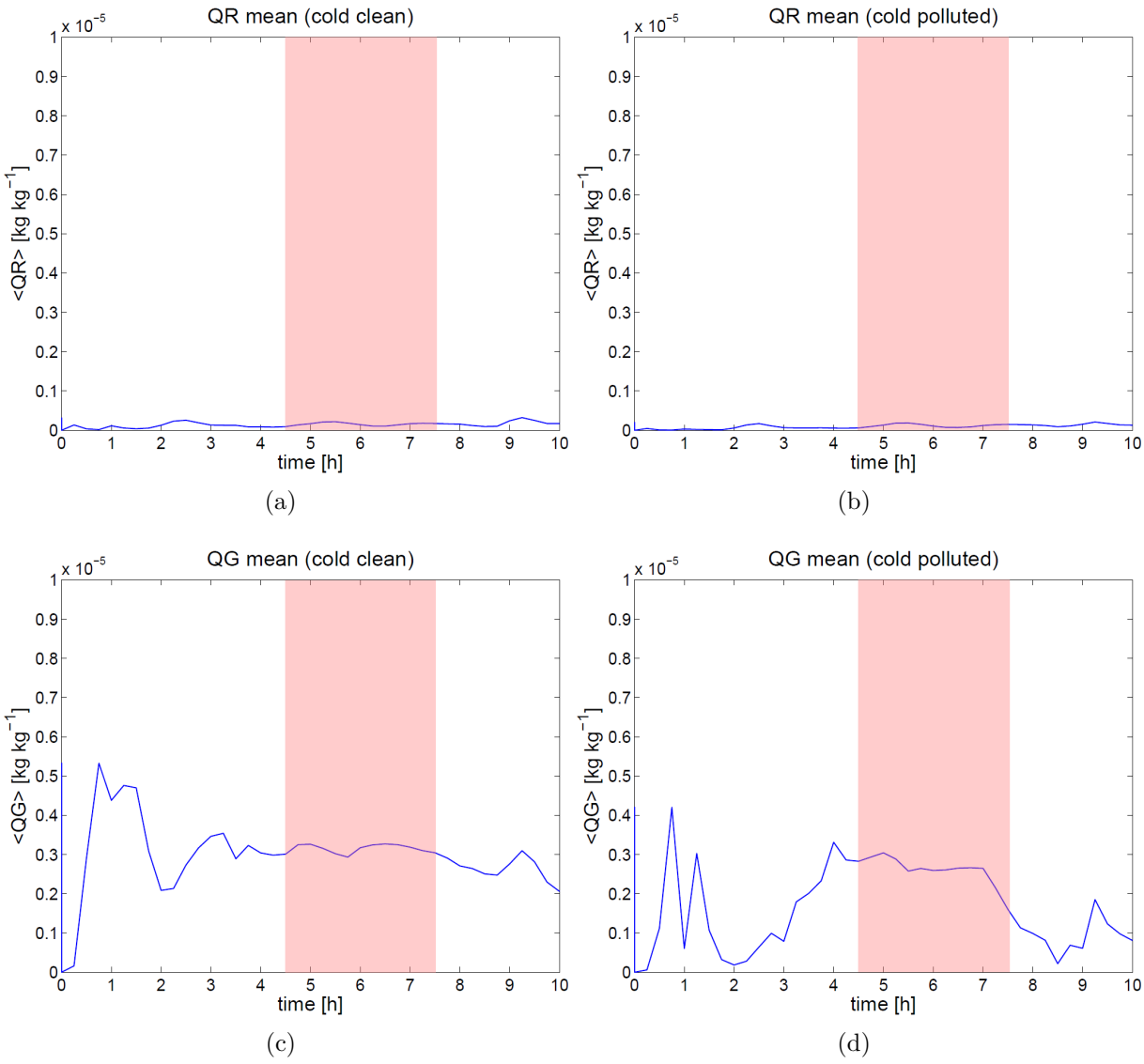

Figure A.5: **Integrated time averages of QR and QG**

A.3 Vertical cross sections

Figure A.6 shows the vertical cross section of the mass mixing ratios of cloud water (top) and cloud ice (bottom) averaged over t=4.5 h to t=7.5 h of SIM_cc and SIM_cp.

The vertical cross section of the mass of aerosols in the accumulation mixed mode and of the mass of black carbon and dust in the accumulation mixed mode are displayed in figure A.7.

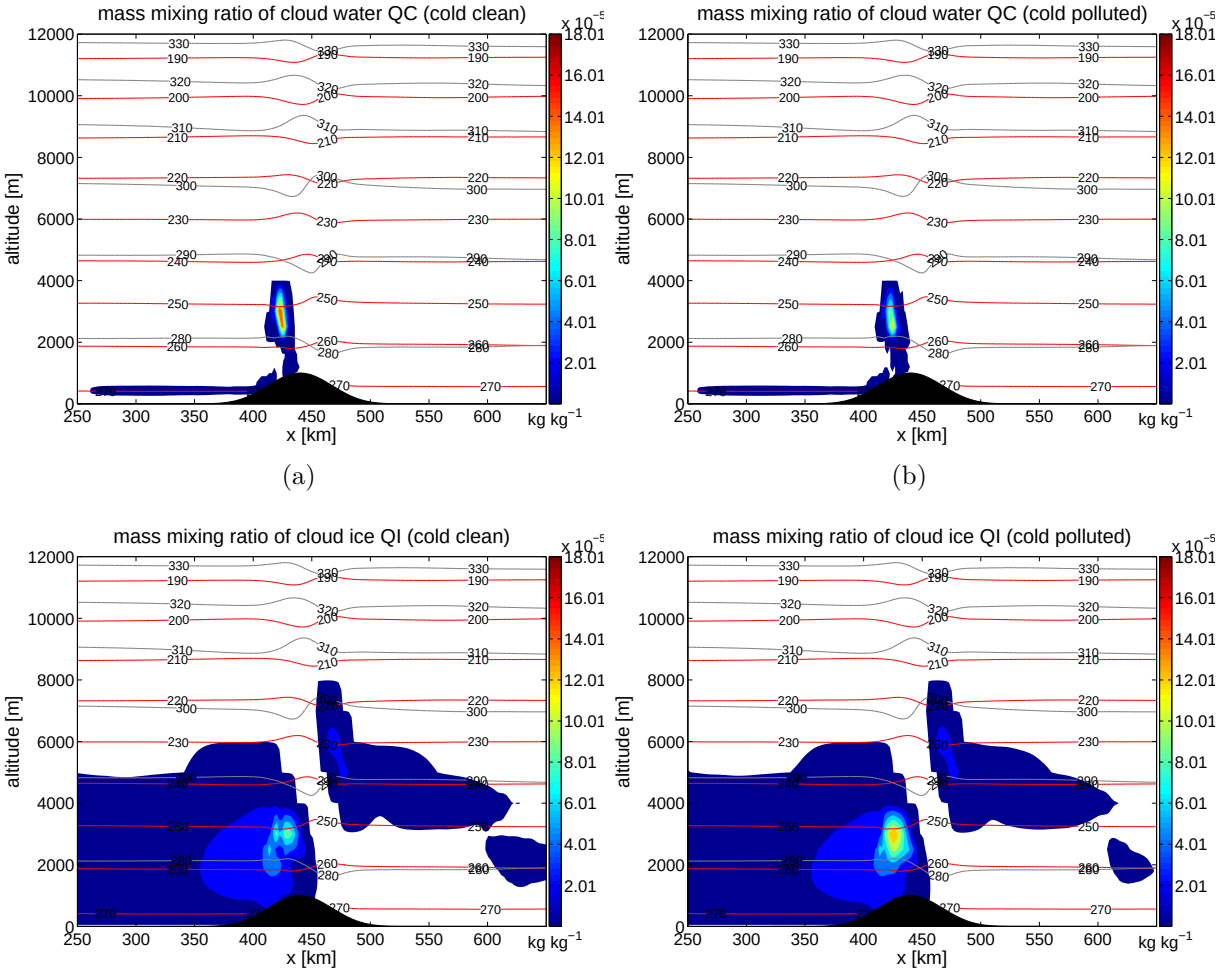

Figure A.6: **Vertical cross section of QC and QI**

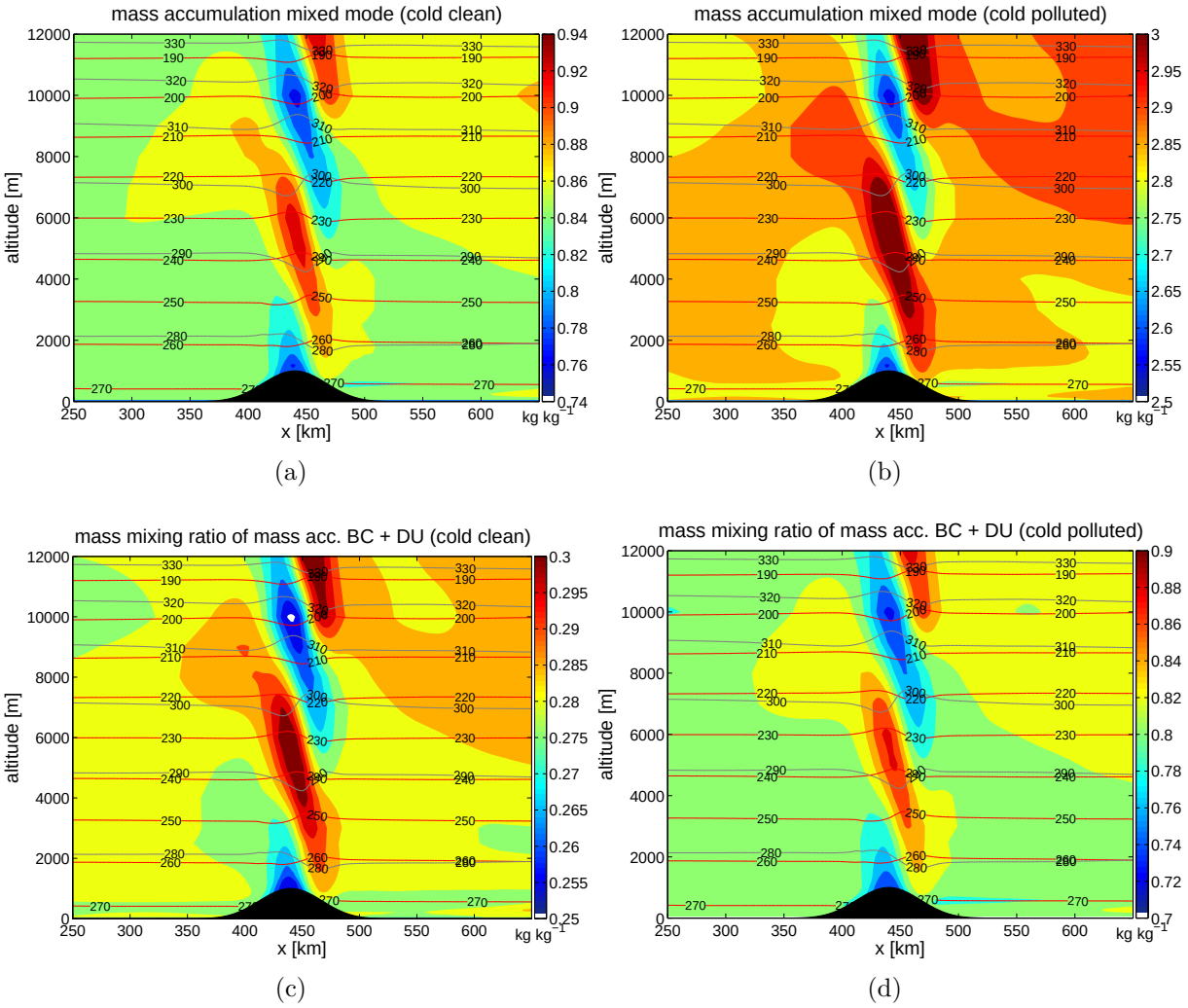

Figure A.7: **Vertical cross section of m_acc and m_acc_BC_DU**

A.4 Activation and freezing rates

Figure A.8 shows the relative difference of the activation and freezing rates. The activation and freezing rates are problematic measures for CCN and IN, respectively, because they strongly depend on supersaturation and temperature.

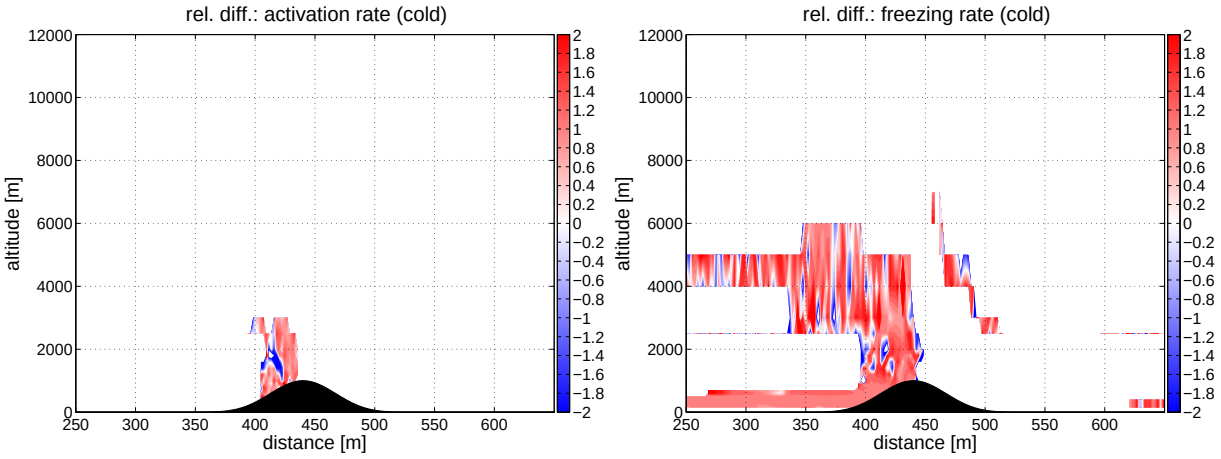

(a) (b)

Figure A.8: **Relative difference of activation and freezing rates**

Bibliography

Albrecht, B. A. (1989), Aerosols, cloud microphysics, and fractional cloudiness, *SCIENCE*, *245*(4923), 1227–1230, doi:10.1126/science.245.4923.1227.

Andreae, M., and D. Rosenfeld (2008), Aerosol–cloud–precipitation interactions. part 1. the nature and sources of cloud-active aerosols, *Earth-Science Reviews*, *89*(1–2), 13 – 41, doi:http://dx.doi.org/10.1016/j.earscirev.2008.03.001.

Bangert, M. J. (2012), Interaction of aerosol, clouds, and radiation on the regional scale, Dissertation, Karlsruher Institut für Technologie.

Borys, R. D., D. H. Lowenthal, and D. L. Mitchell (2000), The relationships among cloud microphysics, chemistry, and precipitation rate in cold mountain clouds, *Atmospheric Environment*, *34*(16), 2593 – 2602, doi:http://dx.doi.org/10.1016/S1352-2310(99)00492-6.

Denman, K., G. Brasseur, A. Chidthaisong, P. Ciais, P. Cox, R. Dickinson, D. Hauglustaine, C. Heinze, E. Holland, D. Jacob, U. Lohmann, S. Ramachandran, P. da Silva Dias, S. Wofsy, and X. Zhang (2007), *Climate Change 2007: The Physical Science Basis. Contribution of Working Group I to the Fourth Assessment Report of the Intergovernmental Panel on Climate Change*, chap. Couplings Between Changes in the Climate System and Biogeochemistry., pp. 499–587, Cambridge University Press, Cambridge, United Kingdom and New York, NY, USA.

Feingold, G., and H. Siebert (2009), Cloud-aerosol interactions from the micro to the cloud scale, in *Clouds in the perturbed climate system: Their relationship to energy balance, atmospheric dynamics, and precipitation*, edited by Heintzenberg, J and Charlson, RJ, pp. 319–338, Conference on Clouds in the Perturbed Climate System, Frankfurt, GERMANY, MAR 02-07, 2008.

Fountoukis, C., and A. Nenes (2005), Continued development of a cloud droplet formation parameterization for global climate models, *Journal of Geophysical Research: Atmospheres (1984–2012)*, *110*(D11).

Herger, N. (2013), Susceptibilities in mixed-phase aerosol-cloud interaction simulated over an alpine transect, Bachelor's thesis, ETH Zurich.

Hoose, C., and O. Möhler (2012), Heterogeneous ice nucleation on atmospheric aerosols: a review of results from laboratory experiments, *Atmospheric Chemistry and Physics*, *12*(20), 9817–9854, doi:10.5194/acp-12-9817-2012.

Hoose, C., U. Lohmann, R. Erdin, and I. Tegen (2008), The global influence of dust mineralogical composition on heterogeneous ice nucleation in mixed-phase clouds, *ERL*, *3*(2), doi:10.1088/1748-9326/3/2/025003.

Koop, T., B. Luo, A. Tsias, and T. Peter (2000), Water activity as the determinant for homogeneous ice nucleation in aqueous solutions, *Nature*, *406*(6796), 611–614.

Lohmann, U. (2002), A glaciation indirect aerosol effect caused by soot aerosols, *Geophysical Research Letters*, *29*(4), 11–1–11–4, doi:10.1029/2001GL014357.

Lohmann, U., and K. Diehl (2006), Sensitivity studies of the importance of dust ice nuclei for the indirect aerosol effect on stratiform mixed-phase clouds, *JAS*, *63*(3), 968–982, doi:10.1175/JAS3662.1.

Lohmann, U., and J. Feichter (2005), Global indirect aerosol effects: a review, *Atmospheric Chemistry and Physics*, *5*(3), 715–737, doi:10.5194/acp-5-715-2005.

Lohmann, U., and F. Lüönd (2012), An introduction to clouds, aerosols and precipitation script for atmospheric physics, ETH Zurich, Institute for Atmospheric and Climate Science, Zurich, Switzerland.

McComiskey, A., and G. Feingold (2012), The scale problem in quantifying aerosol indirect effects, *Atmospheric Chemistry and Physics*, *12*(2), 1031–1049, doi:10.5194/acp-12-1031-2012.

Muhlbauer, A., T. Hashino, L. Xue, A. Teller, U. Lohmann, R. M. Rasmussen, I. Geresdi, and Z. Pan (2010), Intercomparison of aerosol-cloud-precipitation interactions in stratiform orographic mixed-phase clouds, *Atmospheric Chemistry and Physics*, *10*(17), 8173–8196, doi:10.5194/acp-10-8173-2010.

Pruppacher, H. R., and J. D. Klett (1997), *Microphysics of Clouds and Precipitation*, 976 pp., Kluwer Academic Publishers.

Quaas, J., Y. Ming, S. Menon, T. Takemura, M. Wang, J. E. Penner, A. Gettelman, U. Lohmann, N. Bellouin, O. Boucher, A. M. Sayer, G. E. Thomas, A. McComiskey, G. Feingold, C. Hoose, J. E. Kristjansson, X. Liu, Y. Balkanski, L. J. Donner, P. A. Ginoux, P. Stier, B. Grandey, J. Feichter, I. Sednev, S. E. Bauer, D. Koch, R. G. Grainger, A. Kirkevag, T. Iversen, O. Seland, R. Easter, S. J. Ghan, P. J. Rasch, H. Morrison, J. F. Lamarque, M. J. Iacono, S. Kinne, and M. Schulz (2009), Aerosol indirect effects - general circulation model intercomparison and evaluation with satellite data, *ACP*, *9*(22), 8697–8717.

Roe, G. H. (2005), Orographic precipitation, *Annual Review of Earth and Planetary Sciences*, *33*(1), 645–671, doi:10.1146/annurev.earth.33.092203.122541.

Seifert, A., and K. D. Beheng (2006), A two-moment cloud microphysics parameterization for mixed-phase clouds. part 1: Model description, *MAP*, *92*(1-2), 45–66, doi:10.1007/s00703-005-0112-4.

Solomon, S., D. Qin, M. Manning, Z. Chen, M. Marquis, K. Averyt, M.Tignor, and H. Miller (2007), Ipcc, 2007: Climate change 2007: The physical science basis. contribution of working group i to the fourth assessment report of the intergovernmental panel on climate change, Cambridge University Press, Cambridge, United Kingdom and New York, NY, USA.

Sorooshian, A., G. Feingold, M. D. Lebsock, H. Jiang, and G. L. Stephens (2009), On the precipitation susceptibility of clouds to aerosol perturbations, *GRL*, *36*, doi:10.1029/2009GL038993.

Stevens, B., and G. Feingold (2009), Untangling aerosol effects on clouds and precipitation in a buffered system, *NATURE*, *461*(7264), 607–613, doi:10.1038/nature08281.

Twomey, S. (1977), Influence of pollution on shortwave albedo of clouds, *JAS*, *34*(7), 1149–1152, doi:10.1175/1520-0469(1977)034<1149:TIOPOT>2.0.CO;2.

Vogel, B., H. Vogel, D. Bäumer, M. Bangert, K. Lundgren, R. Rinke, and T. Stanelle (2009), The comprehensive model system cosmo-art – radiative impact of aerosol on the state of the atmosphere on the regional scale, *Atmospheric Chemistry and Physics*, *9*(22), 8661–8680, doi:10.5194/acp-9-8661-2009.

Weingartner, E., S. Nyeki, and U. Baltensperger (1999), Seasonal and diurnal variation of aerosol size distributions (10<d<750 nm) at a high-alpine site (jungfraujoch 3580 m asl), *Journal of Geophysical Research: Atmospheres*, *104*(D21), 26,809–26,820, doi:10.1029/1999JD900170.

Zubler, E. M., U. Lohmann, D. Lüthi, C. Schär, and A. Muhlbauer (2011), Statistical Analysis of Aerosol Effects on Simulated Mixed-Phase Clouds and Precipitation in the Alps, *JAS*, *68*(7), 1474–1492, doi:10.1175/2011JAS3632.1.